Simulation and Modification of a Composite Trombe Wall to Adapt to the Climate in Victoria, Canada

by

Zhijie Yin

BEng, Northwestern Polytechnical University, 2012

A Report Submitted in Partial Fulfillment of the Requirements for the Degree of

MASTER OF ENGINEERING

in the

Department of Mechanical Engineering

© Zhijie Yin, 2016
University of Victoria

Supervisory Committee

Simulation and Modification of a Composite Trombe Wall

to Adapt to the Climate in Victoria, Canada

by

Zhijie Yin
BEng, Northwestern Polytechnical University, 2012

Supervisory Committee

Dr. Curran Crawford   Department of Mechanical Engineering
Supervisor

Dr. Phalguni Mukhopadhyaya   Department of Civil Engineering
Departmental Member

Abstract

Supervisory Committee

Dr. Curran Crawford   Department of Mechanical Engineering
Supervisor

Dr. Phalguni Mukhopadhyaya   Department of Civil Engineering
Departmental Member

As one of the passive solar techniques, the composite Trombe wall system stands out for its

ability to provide better indoor thermal comfort for residents. Many experimental and

numerical studies were conducted in the past to investigate its thermal performance in various

climates around the world. However, no research has been done so far to adapt this passive

system to Canada's west coast.

In this project, an existing composite Trombe wall design is studied first with a model

developed in COMSOL Multiphysics® environment. After being validated with published

data, this model is applied with Victoria weather conditions for both cooling and heating

modes. Its insufficient heating ability for the local winter leads to a modification study. By

applying the orthogonal experiment design method, two parametric simulation studies are

conducted to optimize several geometric and thermal dynamic properties of the structure.

Compared to the original design, the modified model achieves better indoor average

temperature stability and less spatial temperature stratification. The results of this study are

fundamental in helping architects or project managers to introduce this bioclimatic design to

Canada's west coast.

Table of Contents

List of Figures

List of Tables

Nomenclature

Acronyms

ANOVA	Analysis of variance
MSE	Mean sum of square of error
MSV	Mean sum of square value
NOLV	Near optimal level value
PC	Percentage contribution
SSV	Sum of square value
TSS	Total sum of square

Symbols

a	Thermal diffusivity	m²/s
A	Area	m²
C	Specific heat capacity	J/kg·°C
C_d	Discharge coefficient	
F_e	Emission factor between two parallel surfaces	
F_z	Buoyancy force	N
g	Acceleration of gravity	m/s²
Gr	Grashof number	
h	Convection coefficient	W/m² °C
H	Height	m
K	Number of factors	
L	Thickness	m

l	Characteristic length	
Le	Number of level	
m	Air mass flow rate	kg/s
M	Mean value of each level of a design factor	
N	Number of experiments conducted	
Nu	Nusselt number	
P	Performance parameter value	
Pr	Prandtl number	
R	Thermal resistance	
R_A	Specific gas constant	
Ra	Rayleigh number	
S	Sum of observations of all experiments	
T	Temperature	K
v	velocity	m/s
W	Width	m
x	Cartesian coordinate	

Greek letters

Φ	Heat flux	kJ/h
β	Volumetric thermal expansion coefficient	1/K
ε	Emissivity	
ζ	Sum of load loss coefficients	
λ	Thermal conductivity	W/m °C
μ	Dynamic viscosity	Pa s

ρ	Density	kg/m³
σ	Stefan–Boltzmann constant	5.674 E-8 W/m² K⁴
τ	Transmissivity	
Υ	Ratio of specific thermal capacity	
φ	Heat flux density	W/m²
δ	Tiny length element	m
ω	Weight for each factor	

Subscripts

amb	Ambiance
avg	Average
bottom	Bottom vent
ch	Chimney
close	Vent closed
cond	Conduction
conv	Convection
env	Environment
f	Fluid
fl	Floor
g	Glazing
gy	Gypsum
i	Insulation
in	Inside surface
m	Mass wall

open	Vent open
out	Outside surface
r	Interior room
ra	Radiation
s	Solar
top	Top vent
v	Vent
w	Wind

Acknowledgement

I would first like to thank my supervisor, Dr. Curran Crawford, for always being patient and supportive whenever I had questions about my research project. As well a heartfelt thank you to the Sustainable System Design Lab group for all the knowledge and fun experiences in and out of the lab. I would also like to acknowledge my friend Ken Streutker for providing me valuable assistance with writing skills in my second language, English. Finally, I must express my gratitude to my parents and my partner for providing me with unfailing support and continuous encouragement throughout my years of study.

Zhijie Yin

Chapter 1   Introduction

1.1 Overview

With passive solar techniques, it is possible to reduce the annual heating and cooling demand of buildings so they meet the passive house standard. According to the Passive House Institute, for a building to be considered a passive house, the space heating energy demand should not exceed 15 *kWh* per square meter per year. [1]. For different climate regions, the passive house principle remains the same, while the specific solution has to be adapted to the region. Among various passive solar systems developed to make use of solar thermal energy, such as solar chimneys [2], solar roofs [3], etcetera, the Trombe wall system stands out for its high efficiency [4] in heating building interiors in the winter time.

A Trombe wall, as shown in Figure 1, is a passive solar building design: a wall is built on the winter sun side of a building with a glass external layer and a high heat capacity internal layer separated by a layer of air [5]. The black surface of the high mass wall absorbs solar energy and heats up. The gained heat is stored in the wall and conducted into the adjacent interior space throughout the day and night. The idea of the Trombe wall is similar to the design of south-facing windows combined with mass floor. Compared to the latter one, the main advantage of Trombe wall is its simplicity and ability to provide better indoor comfort level, as it separates the energy gathering surface from living space. However, it can suffer large heat loss during the night or on cloudy days, or produce excessive heat in the summer time due to its low thermal resistance. Once the stored energy in the mass wall is depleted, a reverse heat flow begins from inside to the outside leading to heat loss from the dwelling.
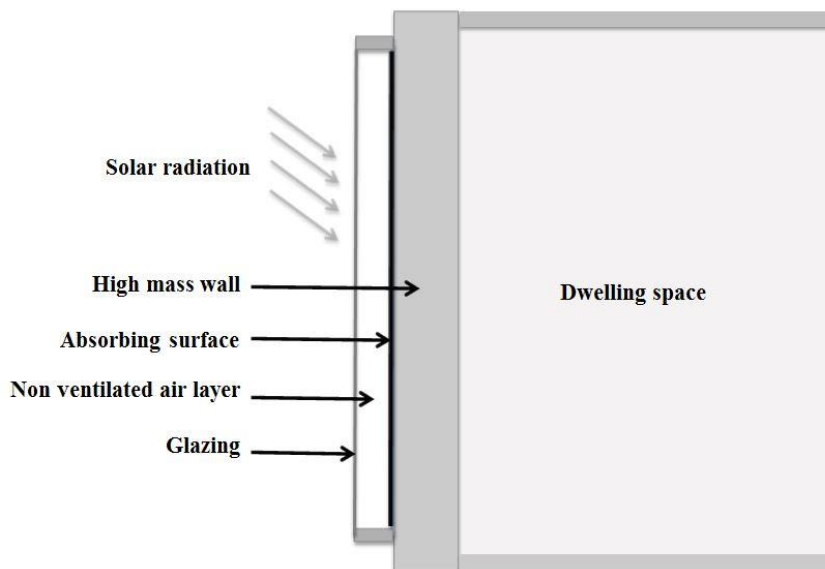
Figure 1: Trombe wall

A solution is to include an insulation panel located at the back of the mass wall. This composite system is called the Trombe-Michel wall [6] as shown in Figure 2. On sunny days, the gained energy in the mass wall is exchanged by convection with the air layer between the mass wall and the insulation panel. Natural circulation occurs in the air gap through buoyancy. The room air is admitted through a lower vent, heated up by convection in the chimney, and discharged back to the room through an upper vent. Meanwhile, the heated insulation wall transfers the remaining heat to the interior by conduction. On cloudy days or at night, the upper and lower vents in the insulating wall are both closed, forming a thermal barrier with the insulating wall to reduce both reverse heat circulation and heat flux going from indoor to outdoor.

Due to the presence of the insulating wall, the air layer and the vents, the composite Trombe wall has several advantages over the classical Trombe wall. It has better heat resistance to keep heat inside in the winter time and avoid overheating in the summer time. Besides, the heat supply can also be controlled by adjusting the air vents.
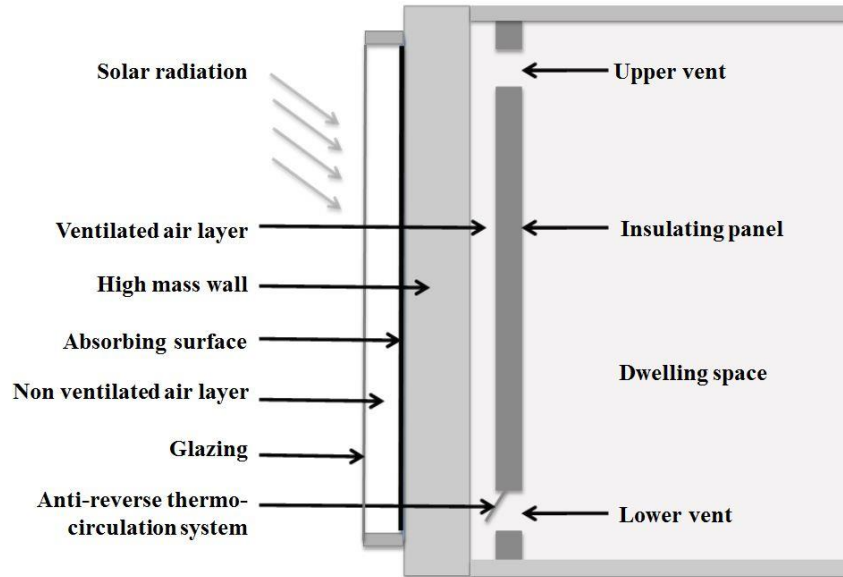
Figure 2: Composite Trombe wall

In this research, the finite element method tool, COMSOL Multiphysics® 5.1 was used to simulate the heat transfer that occurs in the composite Trombe wall system to optimize the temperature field in the interior space. COMSOL Multiphysics® is a FEA simulation software package for various physics and engineering applications, especially for multi-physics. The heat transfer module and the fluid flow module were applied in this project to develop the time dependent model. In the simulation phase, COMSOL's parametric sweep function made it more efficient to conduct multi-factor involved parametric study.

1.2   Objectives

Many experimental structures and numerical models were created for the composite Trombe wall study, but so far no research has been done to adapt this passive heating and cooling system to Canada's west coast. Due to its special climate conditions with mild cloudy winters, it is worth investigating whether the composite Trombe wall will perform well in this location.

This work aims at establishing a clear numerical methodology to quantify the thermal performance of the system and modifying an existing model to achieve indoor thermal comfort with local Victoria, B.C. weather conditions. The objective is to provide guidance for optimizing the passive system generally and understand how different parameters impact the

performance of the system. The research described in this study is comprised of the following activities.

- Creation of a numerical model to simulate the composite Trombe wall performance.

- Validation of numerical simulation using published results.

- Simulation with the original model and Victoria's weather data to evaluate its performance locally.

- Modification of the original model with a two-step parametric design study.

Chapter 2   Model Development

This study is based on Zalewski and his team's research [7]. A measurement experiment was carried out on site in Cadarache, southern France with local weather data. Several simulation studies based on the same wall structure were performed in the following years. [8] - [10]. The same geometric and thermal dynamic parameters of the composite Trombe wall were adopted in this study.

Zalewski's simulation model was developed in one dimension as the original research was focused on the thermal performance of the wall with indoor air temperature simplified as one constant value. In this research, the goal is to study the temperature distribution in the dwelling space and create a thermal comfort environment with minimum temperature stratification. Considering the high calculation cost of a 3D model, and the structure characteristics, a 2D finite element model will be developed for the study.

2.1 Geometric Parameters

The geometric parameters are listed in Table 1 and illustrated in Figure 3.

Table 1.Geometric parameter list

Geometric Parameters			
Wall height	H	2.47	m
Wall width	W	1.34	m
Glass thickness	L_g	0.008	m
Interval between the glazing and the mass wall	L_1	0.03	m
Mass wall thickness	L_m	0.15	m
Interval between the mass wall and the insulating wall	L_2	0.04	m
Height of the orifices of the insulating wall	H_v	0.15	m
Width of the orifice of the insulating wall	W_v	0.6	m
Vertical distance between two orifices	H_0	2	m
Insulating wall thickness	L_i	0.075	m
Gypsum thickness	L_{gy}	0.01	m
Room length	L_r	3.15	m
Vent distance to the floor or ceiling	H_{fl}	0.085	m
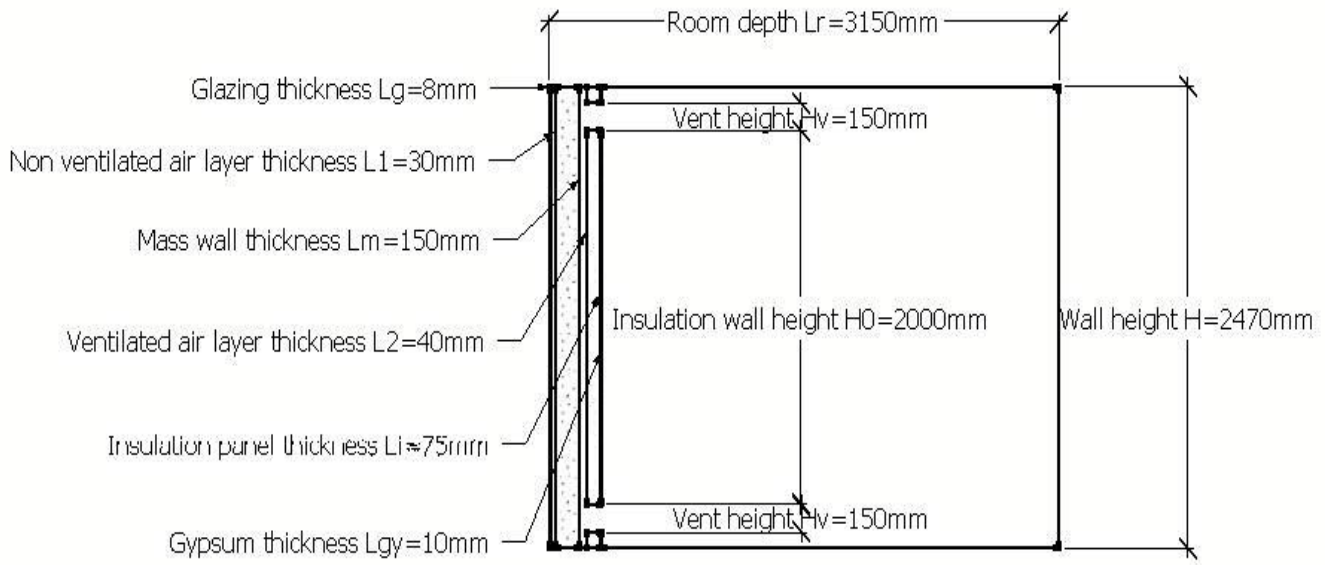
Figure 3: Geometric parameters

2.2 Thermal Dynamic Properties

Most of thermal dynamic properties of each material were referred from the previous simulation models. [8] As to the parameter values of glazing, values are adopted based on the assumption that the glazing is double-paned with conductivity as 0.69 *W/m·℃*, glass density as 2210 *kg/m³* and glass heat capacity as 800 *J/kg·℃*[11]. All the material thermal physical properties are assumed to be independent of temperature, as shown in Table 2.

Table 2.Thermal physical property list

Material Properties									
	Emissivity		Conductivity		Density		Heat Capacity		Transmissivity
	(ε)		λ (W/m·℃)		ρ (kg/m³)		C (J/kg·℃)		τ
Glazing	ε_g	0.9	λ_g	0.69	ρ_g	2210	C_g	800	τ_g	0.81
Mass wall	ε_m	0.9	λ_m	0.81	ρ_m	1900	C_m	949		
Insulating wall	ε_i	0.6	λ_i	0.041	ρ_i	30	C_i	800		
Gypsum	ε_{gy}	0.9	λ_{gy}	0.258	ρ_{gy}	1000	C_{gy}	800		

As this passive solar thermal system involves natural convection, the air properties are assumed to be functions of temperature.

According to John C. Dixon [12], the following air thermal physical properties are formulated:

The thermal conductivity λ is given by

$$\lambda = \frac{0.02646 T_K^{1.5}}{T_K + 245.4 \times 10^{-12/T_K}} \; W/m\,K \tag{2.1}$$

where T_K is the absolute temperature.

The specific thermal capacity c_p at constant pressure is given by the empirical expression

$$c_p = 1002.5 + 275 \times 10^{-6}(T_K - 200)^2 \; J/kg\,K \tag{2.2}$$

The specific heat at constant volume c_V is then

$$c_V = c_p - R_A \tag{2.3}$$

where R_A is the specific gas constant

$$R_A = 287.05 \; J/kg\,K \tag{2.4}$$

The ratio of specific thermal capacity γ is

$$\gamma = \frac{c_p}{c_V} \tag{2.5}$$

The dynamic viscosity μ is given by

$$\mu = \frac{1.458 \times 10^{-6} T_K^{1.5}}{T_K + 110.4} \; Pa\,s \tag{2.6}$$

The volumetric thermal expansion coefficient of air at constant pressure is given by

$$\beta = \frac{1}{T_K} \tag{2.7}$$

2.3 Assumptions and Boundary Conditions

Before processing heat transfer calculations, the following assumptions are made to simplify the model:

- The width of the wall structure is large enough compared with the thickness. As a result, it is taken as a two-dimensional configuration in *x-z* plain.

- The top and bottom wall surfaces are well insulated. Moreover, the heat transfer is only in the form of radiation and conduction for the air gap between the glazing and the mass wall to simplify the calculation. Therefore, heat transfer is one dimensional in the wall. The only temperature gradient exists in the horizontal direction.

- The heat transfer through the glazing and wall is time dependent.

- All surfaces are treated as grey bodies with diffuse reflection and emission.

- Except for the air, all the material thermal physical properties are independent of temperature.

- Air is considered as a nonparticipating medium in radiation heat transfer.

- Air is considered as Newton flow.

- Flow in the system is all laminar flow.

The schematic in Figure 4 shows the applied boundary conditions in different colours. To simplify the model, the horizontal boundaries were set as insulation (black, except the room floor). Ground temperature was applied to the interior room's floor (orange). The exterior surface of the glazing was exposed to both convective heat flux and solar radiation (red). On the internal boundaries presented in magenta, "surface-to-surface" radiation condition was applied in order to simulate greenhouse effect. The remaining internal boundaries were set as continuity (grey).
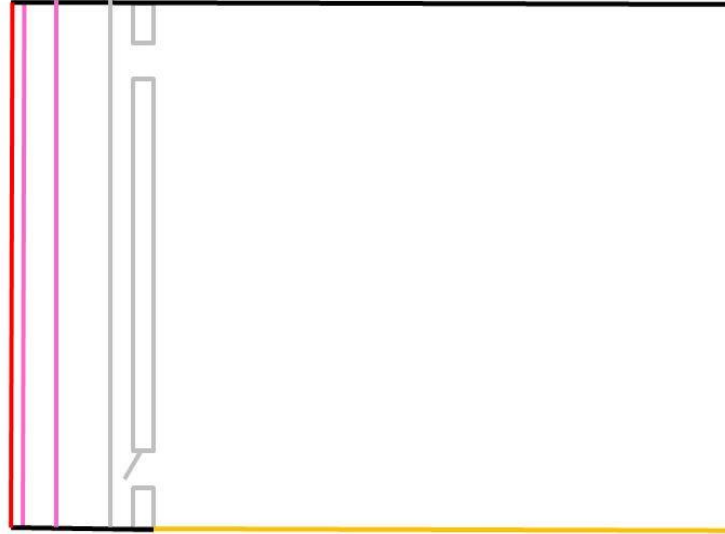
Figure 4: Schematic of boundary conditions

2.4 Thermal Resistance Network

To better understand the general behavior of the composite Trombe wall and identify those design factors that are most critical, the thermal resistance network technique is applied here. It is an electrical analogy of the method used in electrical engineering to analyze the voltage in a circuit. The analog of φ is current, and the analog of the temperature difference ΔT is voltage difference and R is the thermal resistance.

$$\varphi = \frac{\Delta T}{R} \tag{2.8}$$

The analysis is based on the idea that a system consists of different discrete points, knowns as nodes, which are interconnected by the thermal resistance in between. At the boundary, external heat influx and reference temperatures are applied to the relevant nodes. Within the network, the thermal path between two nodes is assumed as one-dimensional. By applying energy balance on each node, the related temperature can be calculated. The equations used are the fundamental heat transfer equations for conduction, convection, and radiation with unit area respectively. The thermal resistances are derived at using the following equations:

2.4.1 Fourier's Law for Heat Conduction in Differential Form

$$\varphi = -\lambda \frac{dT}{dx} \qquad (2.9)$$

where λ is thermal conductivity of the material between the nodes $(W/(m \cdot K))$, $\frac{dT}{dx}$ is the temperature gradient. For a simpler form for the thermal resistance,

$$\varphi = -\lambda \frac{T_1 - T_2}{l} = -\frac{T_1 - T_2}{\frac{l}{\lambda}} \qquad (2.10)$$

$$\text{let } R_{cond} = \frac{l}{\lambda}$$

where l is the distance between nodes.

2.4.2 Newton's Law of Cooling for Heat Convection

$$\varphi = h(T_1 - T_2) = \frac{T_1 - T_2}{\frac{1}{h}} \qquad (2.11)$$

where h is the heat transfer coefficient of the solid node $(W/m^2 \cdot K)$, define

$$R_{conv} = \frac{1}{h} \qquad (2.12)$$

2.4.3 Stefan-Boltzmann Law for Radiation

$$\varphi = \varepsilon\sigma(T_1^4 - T_2^4) \qquad (2.13)$$

where ε is the emissivity of the solid body surface which varies from 0 to 1; σ is called the Stefan-Boltzmann constant of which the value is $5.67 \times 10^{-8} W/(m^2 \cdot K^4)$. Both T_1 and T_2 are absolute temperature.

The correlated thermal resistance of surface radiation is derived from below:

$$\varphi = \varepsilon\sigma(T_1^4 - T_2^4) = \frac{T_1 - T_2}{\frac{1}{\varepsilon\sigma(T_1 + T_2)(T_1^2 - T_2^2)}} \qquad (2.14)$$

$$R_{radiation} = \frac{1}{h_{ra}} = \frac{1}{\varepsilon\sigma(T_1 + T_2)(T_1^2 - T_2^2)} \tag{2.15}$$

where h_{ra} is defined as radiative heat transfer coefficient.

Based on the above assumptions and analogs, a thermal resistance network for the composite Trombe wall is created as demonstrated in Figure 5.
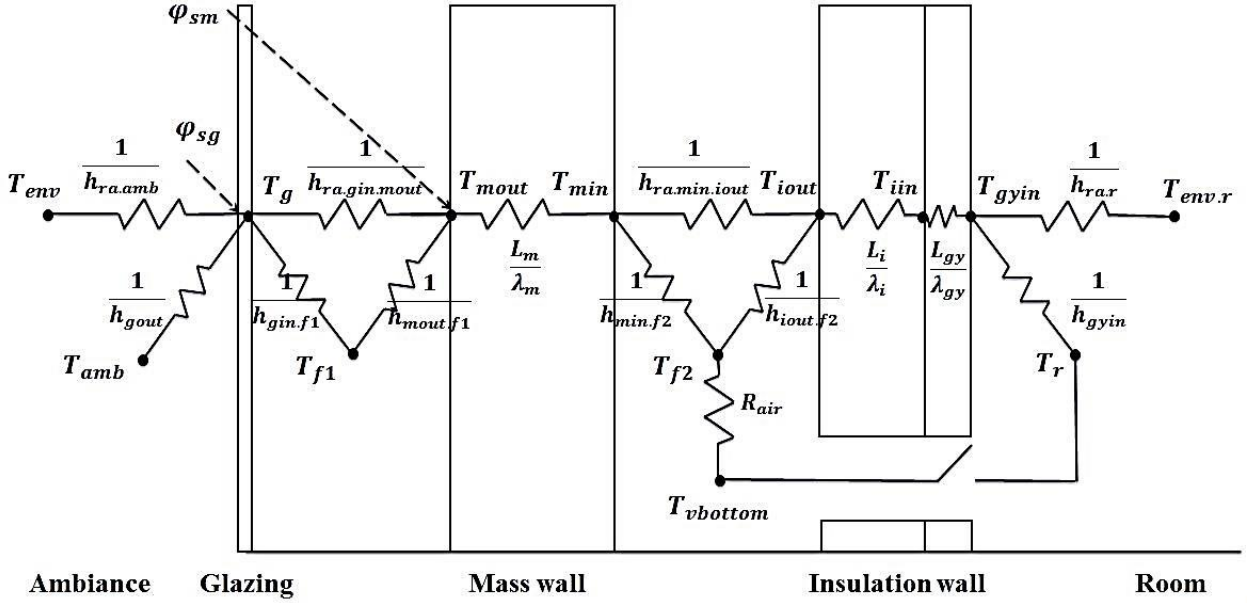
Figure 5: Schematic of thermal resistance network for the composite Trombe wall

As mentioned in the assumption section, the thermal transfer in the wall exists only in horizontal direction. When the upper and lower vents are closed, the network of the wall is a one dimensional model. The inner surface of the gypsum panel is the boundary between the 1D wall model and 2D dwelling space model. When the vents are open, the boundary becomes the inner surface of the mass wall.

This network helps to set up a meaningful finite element model at the early design stage. From the ambiance at the left, to the interior room on the right, heat transfers and distributes by natural convection, conduction and radiation. In the next section, each step of the heat transfer will be investigated in detail.

2.5 Theoretical Calculation

Based on the above assumptions and thermal resistance network, the heat transfer through the composite Trombe wall is analyzed in the following steps.

2.5.1 Energy Balance

From the exterior glazing surface to the interior insulation wall's gypsum surface, the energy balance equations include radiation, convection and conduction. The related convection coefficients and emission factors will be calculated in the next sections.

2.5.1.1 Glazing layer

The thermal balance on the glazing is given by

$$\varphi = h_{gout}(T_{amb} - T_g) + \sigma Fe_{gout.amb}(T_{env}^4 - T_g^4) + \varphi_{sg} \tag{2.16}$$
$$= h_{gin.f1}(T_g - T_{f1}) + \sigma Fe_{gin.mout}(T_g^4 - T_{mout}^4)$$

where h_{gout} is the convention coefficient on the exterior surface of the glazing, T_{amb} is the air ambient temperature, $Fe_{gout.amb}$ is the emission factors for the outside surface of glazing, T_{env} is the environment temperature, φ_{sg} is the solar flux absorbed by the glass, $h_{gin.f1}$ is the convention coefficient on the interior surface of the glazing, T_{f1} is the temperature at the mid-point of the sealed air gap, $Fe_{gin.mout}$ is the emission factor between the inside surface of glazing and the outside surface of the mass wall.

2.5.1.2 Mass wall

The thermal flux through the mass wall is governed by the one-dimensional conduction heat transfer equation:

$$\frac{\partial T}{\partial t} = a_m \frac{\partial^2 T}{\partial x^2} \ (0 < x < L_m) \tag{2.17}$$

where t is time, a_m is the diffusivity of the mass wall:

$$a_m = \frac{\lambda_m}{\rho_m C_{pm}} \quad (0 < x < L_m) \tag{2.18}$$

where L_m is the thickness of the mass wall.

The boundary conditions are given by the energy balance equation at two surfaces (x=0, x=L_m)

At the exterior mass wall surface where x=0, the equation is:

$$-\lambda_m \frac{\partial T}{\partial x}\Big|_{x=0} = h_{mout.f1}(T_{f1} - T_{mout}) + \sigma F e_{gin.mout}(T_{gin}^4 - T_{mout}^4) + \varphi_{sm} \tag{2.19}$$

where $h_{mout.f1}$ is the convention coefficient on the exterior surface of the mass wall; φ_{sm} is the solar heat flux absorbed by the mass wall surface.

At the interior mass wall surface where x=L_m , two cases are studied.

• Vent open:

The energy balance equation at the interior wall surface is given by:

$$-\lambda_m \frac{\partial T}{\partial x}\Big|_{x=L_m} = h_{min.f2.open}(T_{min} - T_{f2}) + \sigma F e_{min.iout}(T_{min}^4 - T_{iout}^4) \tag{2.20}$$

where T_{f2} is the temperature of the air in the chimney between the mass wall and the insulation wall; $h_{min.f2.open}$ is the convention coefficient on the interior surface of the mass wall with open vents; $F e_{min.iout}$ is the emission factors between the inside surface of the mass wall and the outside surface of the insulating wall.

• Vent closed:

$$-\lambda_m \frac{\partial T}{\partial x}\Big|_{x=L_m} = h_{min.f2.close}(T_{min} - T_{f2}) + \sigma F e_{min.iout}(T_{min}^4 - T_{iout}^4) \tag{2.21}$$

where $h_{min.f2.close}$ is the convention coefficient on the interior surface of the mass wall with closed vents.

2.5.1.3 Air chimney between the mass wall and the insulation wall

In the case of open vents, a thermal circulation of air through the chimney is generated when the average air temperature in the chimney is higher than the indoor temperature.

The thermal energy transferred to the air is given by:

$$h_{min.f2}(T_{min} - T_{f2}) = h_{iout.f2}(T_{f2} - T_{iout}) + \varphi_{ch} \tag{2.22}$$

where $h_{iout.f2}$ is the convection coefficient on the outside surface of the insulating wall; T_{f2} is the average temperature of the air flow in the chimney. By assuming that the air temperature varies linearly along the wall height, T_{f2} is given by:

$$T_{f2} = \frac{T_{vtop} + T_{vbottom}}{2} \tag{2.23}$$

where T_{vtop} is the air outlet temperature from the chimney; $T_{vbottom}$ is the dwelling air temperature at the bottom vent.

On the right hand side of energy balance equation, φ_{ch} is the thermal energy transported by the air towards the upper vent, determined by

$$\varphi_{ch} = \frac{mC_{f2}(T_{vtop} - T_{vbottom})}{A_m} \tag{2.24}$$

where A_m is the mass wall area, m is the air mass flow rate, given by:

$$m = \rho_{f2} A_v v_{f2} \tag{2.25}$$

where A_v is the vent area, v_{f2} is the average speed of the air mass flow in the chimney, given by Equation (2.26) [13]

$$v_{f2} = C_d \sqrt{\frac{gH(T_{vtop} - T_{vbottom})}{T_{vtop} + T_{vbottom}}} \tag{2.26}$$

where g is the acceleration of gravity, H is the vertical distance between two vents, C_d is the discharge coefficient, determined by

$$C_d = \sqrt{\frac{2}{\zeta}} \tag{2.27}$$

ζ is the sum of load loss coefficients. Assuming that the friction losses are mostly due to the flow through the vents located at the top and bottom, ζ is given by Equation (2.28)

$$\zeta = \zeta_{bottom} \frac{\rho_{f2}}{\rho_{vbottom}} (\frac{A_{ch}}{A_v})^2 + \zeta_{top} \frac{\rho_{f2}}{\rho_{vtop}} (\frac{A_{ch}}{A_v})^2 \qquad (2.28)$$

where A_{ch} is the chimney section area, $\rho_{vbottom}$ and ρ_{vtop} are the air density at the average temperature $T_{vbottom}$ at the bottom vent and T_{vtop} at the upper vent respectively;

ζ_{bottom} and ζ_{top} are the load loss coefficients at the bottom and top vent respectively. According to the 2001 ASHRAE Handbook [14], when air flows from room to vent, the loss coefficient

$$\zeta_{bottom} = 0.5 \qquad (2.29)$$

when air flows from vent to room (abrupt exit), the loss coefficient

$$\zeta_{top} = 1 \qquad (2.30)$$

2.5.1.4 Insulation wall

The thermal flux through the insulation wall is governed by the one-dimensional conduction heat transfer equation

$$\frac{\partial T}{\partial t} = a_i \frac{\partial^2 T}{\partial x^2} \ (0 < x < L_i) \qquad (2.31)$$

where a_i is the diffusivity of the insulation wall:

$$a_i = \frac{\lambda_i}{\rho_i C_{pi}} \ (0 < x < L_i) \qquad (2.32)$$

where L_i is the thickness of the insulation wall.

The boundary conditions are given by the energy balance equation at two surfaces (x=0, x=L_i)

At x=0, two cases are studied.

- Vent open:

The energy balance equation at the exterior insulation surface is given by:

$$-\lambda_i \frac{\partial T}{\partial x}|_{x=0} = h_{iout.f2.open}(T_{iout} - T_{f2}) + \sigma Fe_{min.iout}(T_{iout}^4 - T_{min}^4) \qquad (2.33)$$

- Vent closed:

The energy balance equation at the exterior insulation surface is given by:

$$-\lambda_i \frac{\partial T}{\partial x}\big|_{x=0} = h_{iout.f2.close}(T_{iout} - T_{f2}) + \sigma Fe_{min.iout}(T_{iout}^4 - T_{min}^4) \tag{2.34}$$

At $x=L_i$, this is the interface between the insulation wall and gypsum layer,

$$\frac{\partial T}{\partial t} = a_{igy} \frac{\partial^2 T}{\partial x^2} \ (-\delta x < x < \delta x) \tag{2.35}$$

where a_{igy} is the average diffusivity of the insulation material and the gypsum, δx is a tiny length element.

2.5.1.5 Gypsum layer

$$\frac{\partial T}{\partial t} = a_{gy} \frac{\partial^2 T}{\partial x^2} \ (0 < x < L_{gy}) \tag{2.36}$$

where a_{gy} is the diffusivity of the gypsum layer,

$$a_{gy} = \frac{\lambda_{gy}}{\rho_{gy} C_{pgy}} \ (0 < x < L_{gy}) \tag{2.37}$$

The boundary condition at the inner surface of gypsum is given by the energy balance equation:

$$-\lambda_{gy} \frac{\partial T}{\partial x}\big|_{x=L_{gy}} = h_{gyin}(T_{gyin} - T_r) + \sigma Fe_{gy.r}(T_{gyin}^4 - T_{env.r}^4) \tag{2.38}$$

where h_{gyin} is the convection coefficient on the inside surface of the gypsum panel; $Fe_{gy.r}$ is the emission factor between the inside surface of the gypsum panel and the interior room.

2.5.1.6 Convection in the dwelling area

The governing equations for the convection heat transfer in the room are mass, momentum and energy conservation equations in two dimensions.

$$\frac{D\rho}{\partial t} + \frac{\partial(\rho u)}{\partial x} + \frac{\partial(\rho v)}{\partial z} = 0 \tag{2.39}$$

$$\rho\left(\frac{\partial u}{\partial t} + u\frac{\partial u}{\partial x} + v\frac{\partial u}{\partial z}\right) = F_x - \frac{\partial p}{\partial x} + \mu(\frac{\partial^2 u}{\partial x^2} + \frac{\partial^2 u}{\partial z^2})$$

$$\rho\left(\frac{\partial v}{\partial t} + u\frac{\partial v}{\partial x} + v\frac{\partial v}{\partial z}\right) = F_z - \frac{\partial p}{\partial z} + \mu(\frac{\partial^2 v}{\partial x^2} + \frac{\partial^2 v}{\partial z^2})$$

$$\frac{\partial T}{\partial t} + u\frac{\partial T}{\partial x} + v\frac{\partial T}{\partial z} = \frac{\lambda}{\rho C_p}(\frac{\partial^2 T}{\partial x^2} + \frac{\partial^2 T}{\partial z^2})$$

where F_z in the momentum equation is the buoyancy force, μ is the dynamic viscosity.

2.5.2 Convection Coefficients

2.5.2.1 Outside surface of the glazing $\boldsymbol{h_{gout}}$

The average convection coefficient due to wind on the glazing [15]:

$$h_{gout} = 5.7 + 3.8v_w \qquad (2.40)$$

where v_w is the wind speed gained from local meteorological data files.

2.5.2.2 Inside surface of the glazing $\boldsymbol{h_{gin.f1}}$, outside surface of the mass wall $\boldsymbol{h_{mout.f1}}$

In this case, heat transfers by natural convection across vertical air layer in an enclosed space formed by the inside surface of glazing, the outside surface of the mass wall and the two ends.

Suppose the heat transferred by convection is Φ, the temperature difference between the two walls is ΔT_1, the temperature difference between the wall surface and the fluid in ΔT_2. Based on energy conservation,

$$\Phi = h_{gin.mout}\Delta T_1 = h_{gin.f1}\Delta T_2 \qquad (2.41)$$

Neglecting the slight differences between $h_{gin.f1}$ and $h_{mout.f1}$, the mid-fluid must be at a temperature midway between that of the two surfaces. Therefore,

$$\Delta T_1 = 2\ \Delta T_2 \qquad (2.42)$$

and

$$h_{gin.mout} = \frac{1}{2}h_{gin.f1} = \frac{1}{2}h_{mout.f1} \qquad (2.43)$$

where $h_{gin.f1}$ is given by

$$h_{gin.f1} = \frac{Nu\lambda_{f1}}{L_{f1}} \tag{2.44}$$

where L_{f1} is the thickness of the enclosed air gap, Nu is the Nusselt number.

The temperatures of the inside glazing surface T_{gin}, and the outside mass wall surface T_{mout} are assumed to be uniform respectively, and the $z = 0$ and $z = H$ ends to be insulated. The average temperature of the fluid:

$$T_{f1} = \frac{T_{gin} + T_{mout}}{2} \tag{2.45}$$

is the characteristic temperature for the Nusselt number Nu, which is determined from [16]:

$$Nu = Max\{1, 0.288Ra_l^{1/4}, 0.039Ra_l^{1/3}\} \tag{2.46}$$

where the characteristic length, l, is the distance between parallel surfaces L_{f1}.

Ra is Rayleigh number,

$$Ra = GrPr \tag{2.47}$$

where Gr is Grashof number, given by:

$$Gr = \frac{\beta_{f1}g\rho_{f1}^2 L_{f1}^3 (T_{mout} - T_{f1})}{\mu^2} \tag{2.48}$$

Pr is Prandtl number, given by:

$$Pr = \frac{\mu C_{f1}}{\lambda_{f1}} \tag{2.49}$$

2.5.2.3 Within the chimney $h_{min.f2}$, $h_{iout.f2}$ and $h_{min.iout}$

- Vents open

In the case of open vents, the chimney is an air channel. There will be fluid flow and thermal transfer in vertical direction, which means the model from this point switches to two dimension. The convection coefficients are the average value for each surface.

The correlated convection coefficients are given by:

$$h_{min.f2.open} = h_{iout.f2.open} = \frac{Nu\lambda_{f2}}{H} \tag{2.50}$$

where the characteristic length is the wall height and the Nusselt number is determined by Equation (2.51) [17]:

$$Nu = 0.12 \, Pr^{1/3} Gr^{1/3} \tag{2.51}$$

The Grashof number is given by:

$$Gr = \frac{\beta_{f2} g \rho_{f2}^2 H^3 (T_{vtop} - T_{vbottom})}{\mu^2} \tag{2.52}$$

- Vents closed

In the case of closed vents, as mentioned in the assumption section, the buoyancy driven flow in the narrow air gap is neglectable. Therefore, the model in this area is still one dimensional.

Same as the case of $h_{gin.mout}$, $h_{min.iout}$ is given by:

$$h_{min.iout} = \frac{1}{2} h_{min.f2.close} = \frac{1}{2} h_{iout.f2.close} \tag{2.53}$$

where

$$h_{min.f2.close} = \frac{Nu\lambda_{f2}}{L_{f2}} \tag{2.54}$$

where the characteristic length L_{f2} is the thickness of the channel.

$$Nu = Max\{1, 0.288Ra_l^{1/4}, 0.039Ra_l^{1/3}\} \tag{2.55}$$

Rayleigh number,

$$Ra = GrPr \tag{2.56}$$

Where

$$Gr = \frac{\beta_{f2} g \rho_{f2}^2 L_{f2}^3 (T_{min} - T_{f2})}{\mu^2} \tag{2.57}$$

$$Pr = \frac{\mu C_{f2}}{\lambda_{f2}} \tag{2.58}$$

2.5.2.4 Inside surface of the gypsum wall h_{gy}

Compared to the chimney channel, the room is an infinite space. Therefore, the coefficient for the natural convection is determined by [18]:

$$Nu_H = 0.59(Gr_H Pr)^{1/4} \quad 1.43 \times 10^4 < Gr_H < 3 \times 10^9 \quad (2.59)$$
$$Nu_H = 0.0292(Gr_H Pr)^{0.39} \quad 3 \times 10^9 < Gr_H < 2 \times 10^{10}$$
$$Nu_H = 0.11(Gr_H Pr)^{1/3} \quad Gr_H > 2 \times 10^{10}$$

where

$$Gr_H = \frac{\beta_{fr} g \rho_{fr}^2 H^3 (T_{gy} - T_r)}{\mu^2} \quad (2.60)$$

$$Pr = \frac{\mu C_{fr}}{\lambda_{fr}} \quad (2.61)$$

2.5.3 Emission Factors

For any two parallel surfaces n and m, the emission factor $Fe_{n,m}$ is

$$Fe_{n,m} = \frac{1}{\frac{1}{\varepsilon_n} + \frac{1}{\varepsilon_m} - 1} \quad (2.62)$$

where ε_n and ε_m are surface emissivity for n and m respectively.

2. 6 Meteorological Data

To validate the model, weather data from Carpentras in southern France (latitude 44.05°N, longitude 5.03° E) is used. The validation simulation was carried out for 48 hours in February. Figure 6 and Figure 7 show the meteorological data in France.
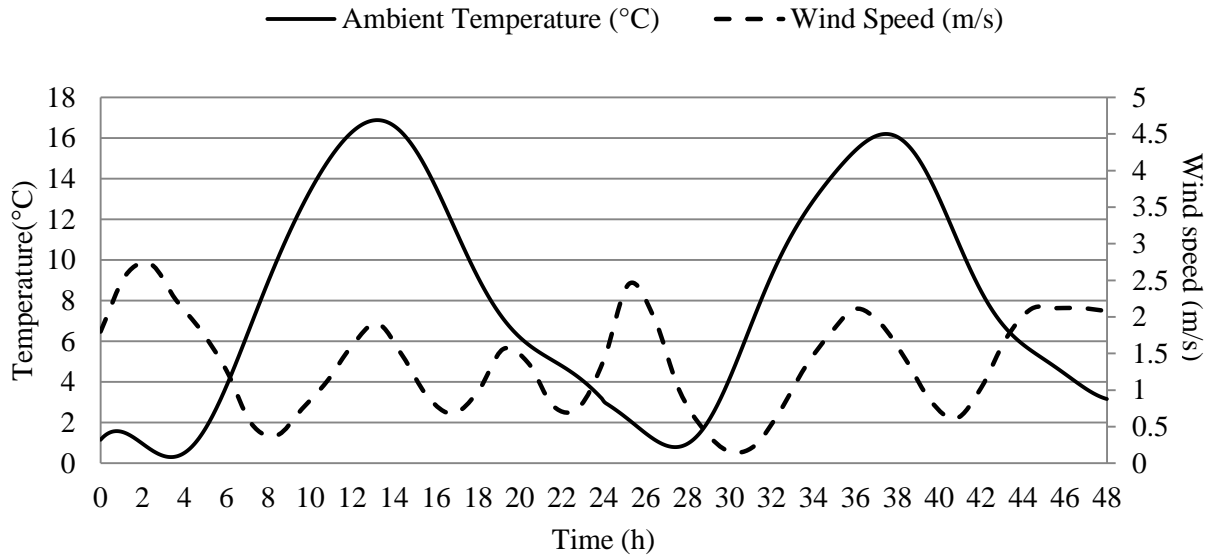
Figure 6: Meteorological data-temperature and wind speed for Carpentras, France
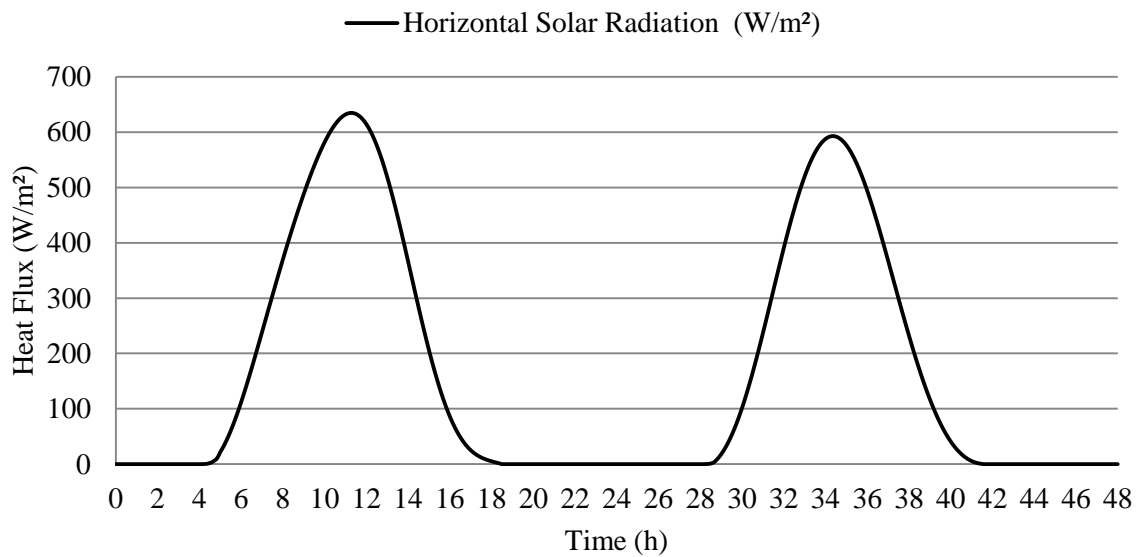
Figure 7: Meteorological data-solar heat flux for Carpentras, France

2.7 Mesh

The structured, non-uniform triangle mesh is generated in COMSOL Multiphysics® 5.1 for validation and numerical simulation. The complete mesh consists of 10429 elements. The quality of the mesh is evaluated before the simulation. The value of the mesh element quality

is based on the ratio of the inscribed and circumscribed circles' radii for the simplex corresponding to each corner of the element. [19] It ranges between 0 and 1, where 0 means a degenerated element and 1 represents the best possible element.

Based on the evaluation of the mesh generated for this model, the average mesh element quality is 0.73 with the minimum element quality value of 0.05.

Figure 8 shows the mesh and its quality distribution in the 2D model.
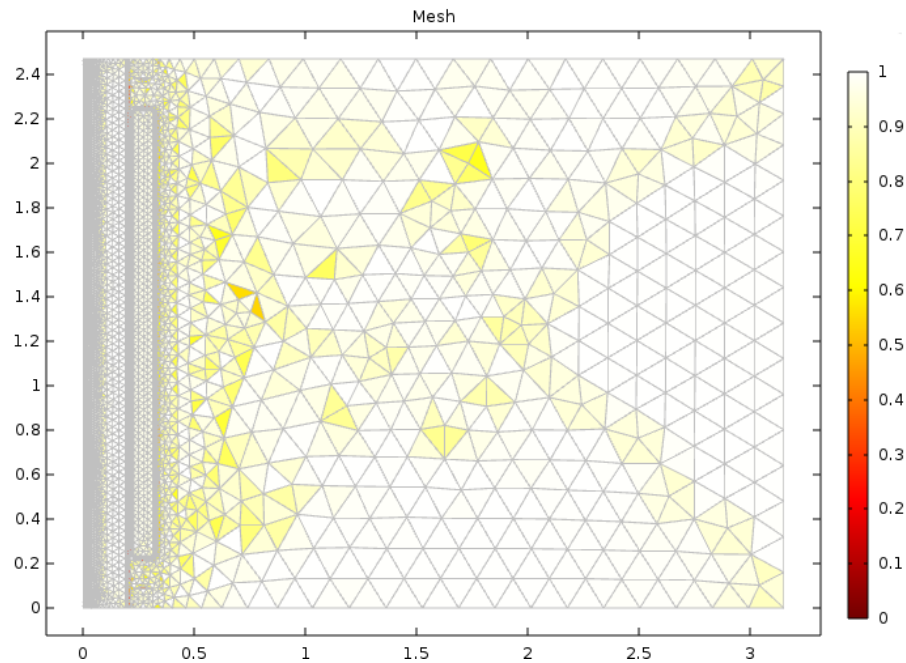
Figure 8: Mesh quality spatial distribution

Figure 9 shows the mesh quality statistically. Less than 8% of the elements have a value lower than 0.1. Usually the value of minimum element quality is preferred greater than 0.1 [20]. In this case, the minimum value of 0.05 generated is due to the boundary layer next to the vertical inside walls which consist of long rectangular elements, leading to a relatively smaller ratio of the inscribed and circumscribed circles radii. Besides the boundary layers, the rest of the elements have really good mesh quality.
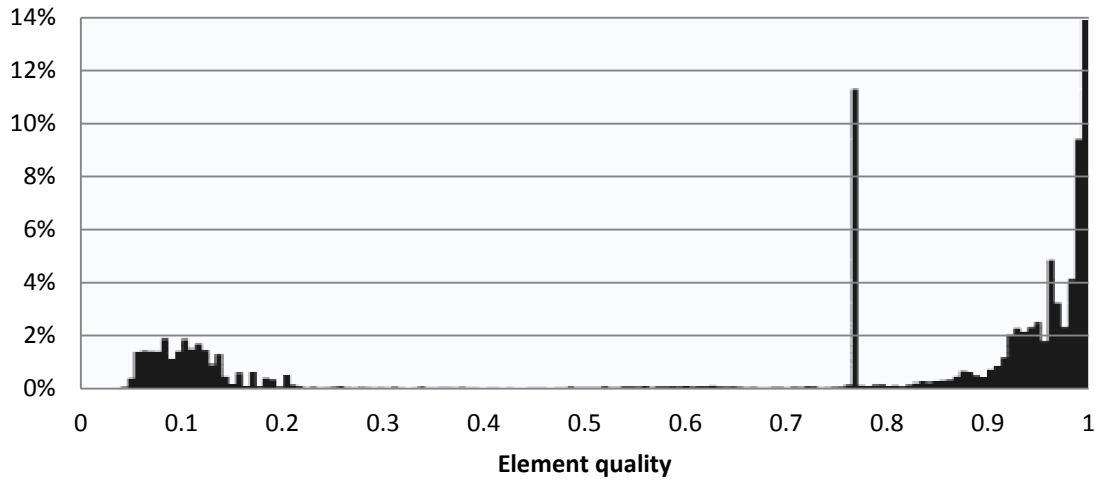
Figure 9: Mesh quality statistic distribution

2.8 Numerical Solver

As this model is a time dependent study, a time-dependent solver is used. In COMSOL, the implicit time-dependent solver is used to solve the ordinary differential equations (ODE). It applies variable-order variable-step-size backward differentiation formulas (BDF). BDF methods have been used for a long time and are known for their stability [19].

Chapter 3   Validating Model

The model is generated based on Dr. Zalewski's papers. In order to validate this 2D model, the indoor temperature is set to 19°C throughout the simulation, same setting as the published model [9]. The geometries, material properties, boundary conditions and weather files are set identically to the published model. The COMSOL simulation results are compared with the published results gained by both experimental and numerical studies. In the structure, the external surface of the mass wall is where the most solar radiation is captured, while the internal surface of the insulation wall is where the input heat goes into the dwelling space. Therefore, temperature probes are placed on these two surfaces to compare with Zalewski's results. In some other literatures [8] [9], the thermal flux through the wall is also computed.

For the sake of clarity, the simulation has been limited to 2 days. According to Zalewski, weather data of February 26th and 27th are used. To minimize the transient effect due to the initial conditions, before starting the simulation, two pre-run simulations with the first day's weather data are conducted.

Figure 10 and Figure 11 show the temperature at the external surface of the mass wall and the internal surface of the insulation wall respectively. The shade area in the plot indicates the night hours (without solar radiation). The results show that good agreement between the COMSOL model and the published model is achieved. The deviation between the mass wall outside surface temperature is less than 3.4% with 2.05°C maximum difference at the 37th hour and the maximum deviation for the inside insulation wall is less than 0.03% with 0.06°C maximum difference at the 32nd hour.

COMSOL modeling doesn't allow setting value to the transmissivity of glazing. The extra solar radiation which should have been absorbed and reflected by glazing is absorbed by the mass wall. This may cause the slightly higher wall temperature in its model.

T_outmasswall from model (^{0}C) — — T_outmasswall from published data (^{0}C)
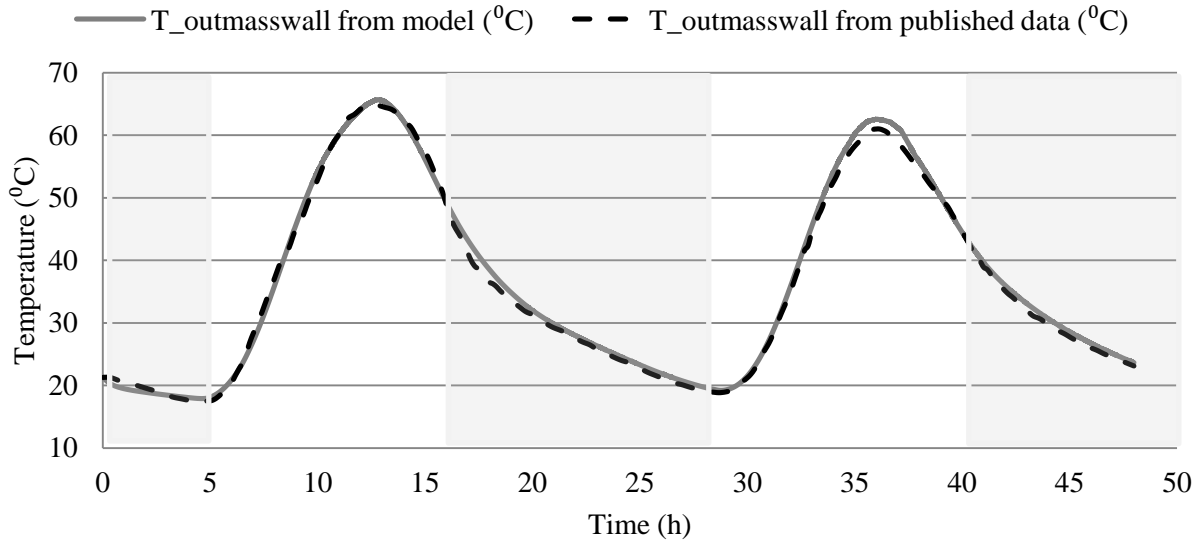
Figure 10: Temperature at the external surface of the mass wall

T_ininsulwall from model (^{0}C) — — T_ininsulwall from published data (^{0}C)
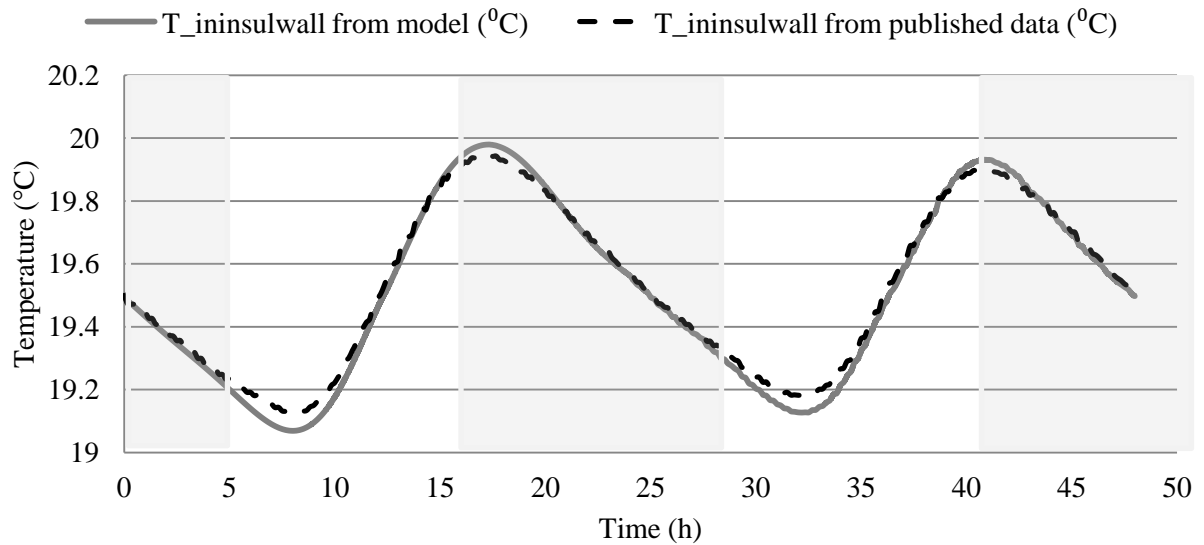
Figure 11: Temperature at the internal surface of the insulation wall

For a visual check on the model validity, the thermal and velocity profiles of the structure at 08:00, 12:00 and 16:00 are shown in Figure 12 and Figure 13 respectively. Since COMSOL doesn't allow setting a domain volumn at a constant single temeprature value, the room space at 19°C is represented by an open boundary "wall" close to insulation wall at 19°C on the right

end. In each plot, from left (the ambience) to right (the dwelling space), the layers are glazing, sealed air gap, mass wall, air channel, insulation wall with vents, room space.
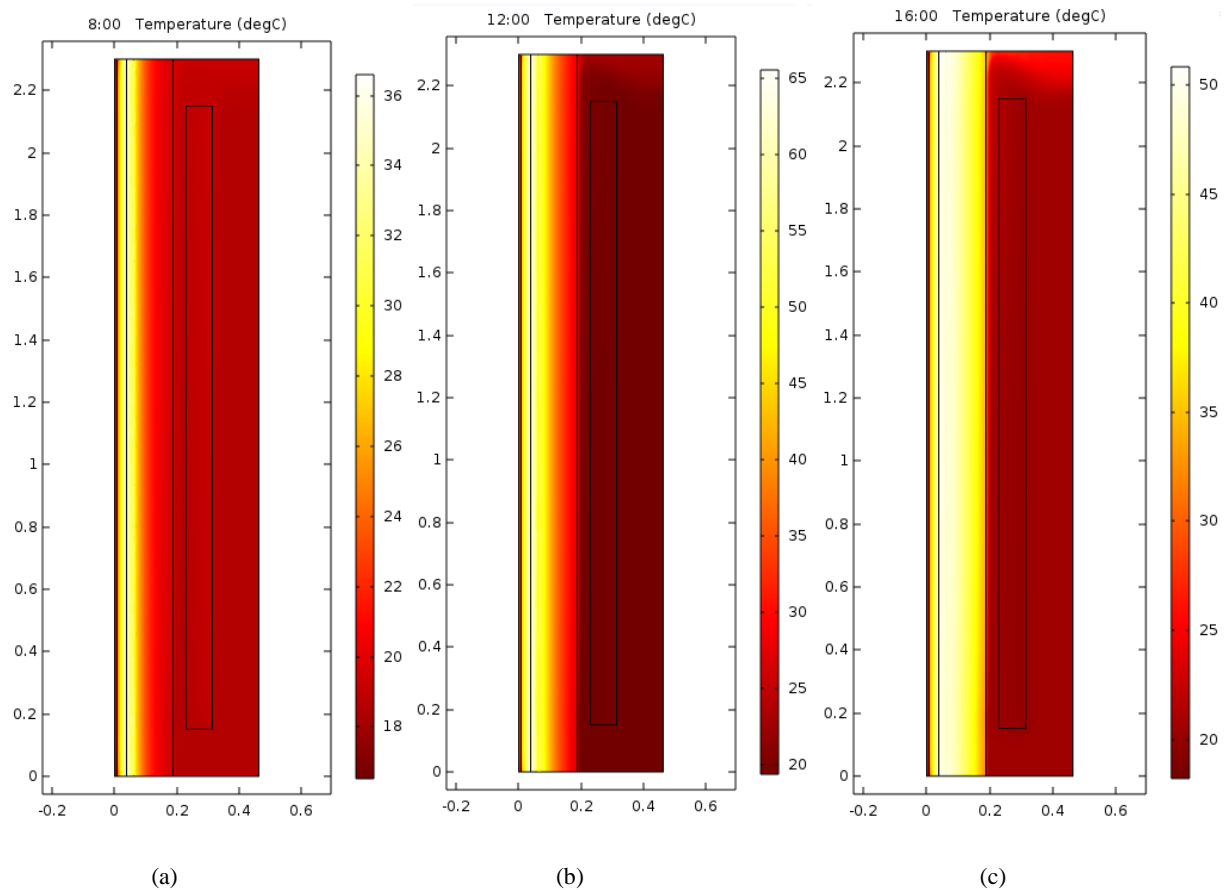
Figure 12: Thermal profile of the wall at 08:00(a), 12:00(b), 16:00(c)

In Figure 12, solar heat collecting and thermal storage function of the Trombe wall is demonstrated. At 8:00, the exterior surface of the mass wall heats up first with the morning sun and the wall starts charging. During the day, its temperature keeps rising while heat travels into the room. At 16:00, the mass wall is fully charged and the air in the channel keeps transfering heat into the room. The corelated air flow velocity profiles are shown in Figure 13. Both the thermal map and the buoyancy driven flow through the vents confirms the validity of the model.
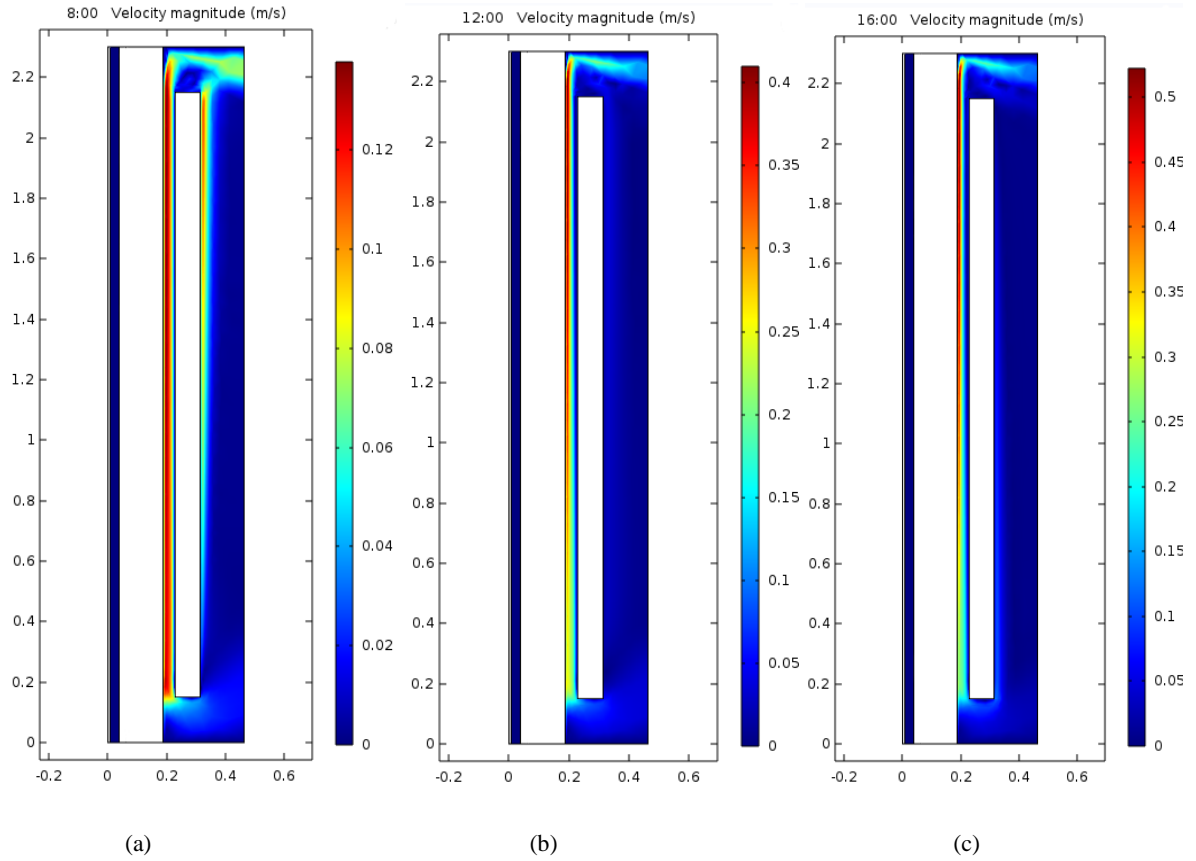
Figure 13: Velocity profile of the wall at 08:00(a), 12:00(b), 16:00(c)

Chapter 4   Simulation for Model Evaluation

Based on the validated model, the performance of the composite Trombe wall will be evaluated with the weather data from Victoria, Canada. Accordingly, the model will be modified to achieve the best dwelling living condition under the local climate.

Victoria has a mild warm Mediterranean climate with rainy winters and sunny summers [21]. The average daily high and low temperatures in winter are 8°C and 4°C respectively. The summer average high temperature is 20°C and low of 11°C. As the second sunniest city in British Columbia, Victoria has an average of 2,193 hours of bright sunshine annually [22]. These climate conditions make it possible to adopt composite Trombe walls in this area to reduce building energy consumption.

In order to decide the structure's heating and cooling ability, the typical weather data of winter solstice day (22nd December) and summer solstice day (21st June) is chosen. Considering the structural thermal delay phenomenon, the day before and after the solstice days are added. These weather data of a typical meteorological year is generated based on the past ten years' weather record, provided by Weather Analytics®.

4.1 Heating Season

Figure 14 and Figure 15 show the winter weather data (December 21-23) for heating season simulation. Within the three days, the ambient temperature ranges from 1°C to 8°C with fairly low solar radiation during the day and higher wind speed at night.
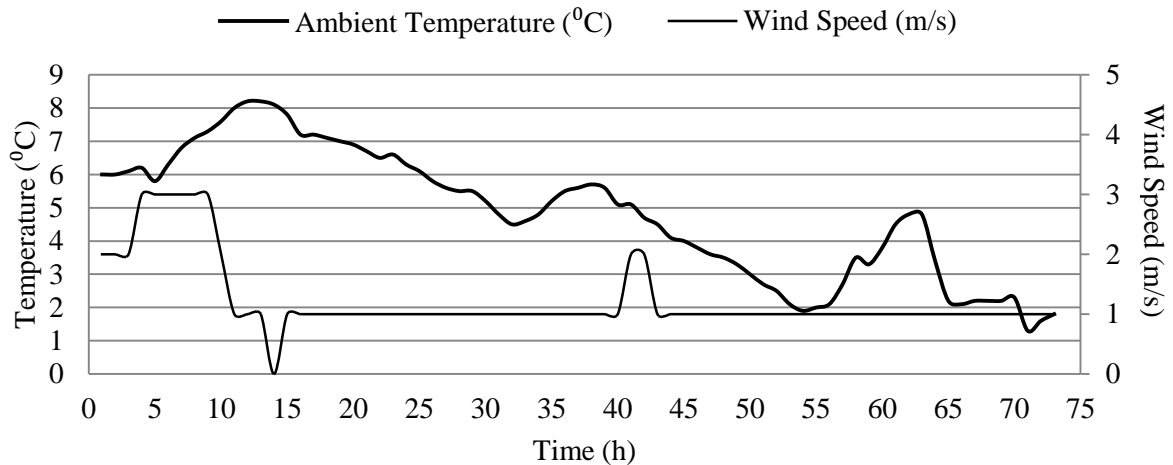
Figure 14: Winter meteorological data-temperature and wind speed for Victoria, Canada
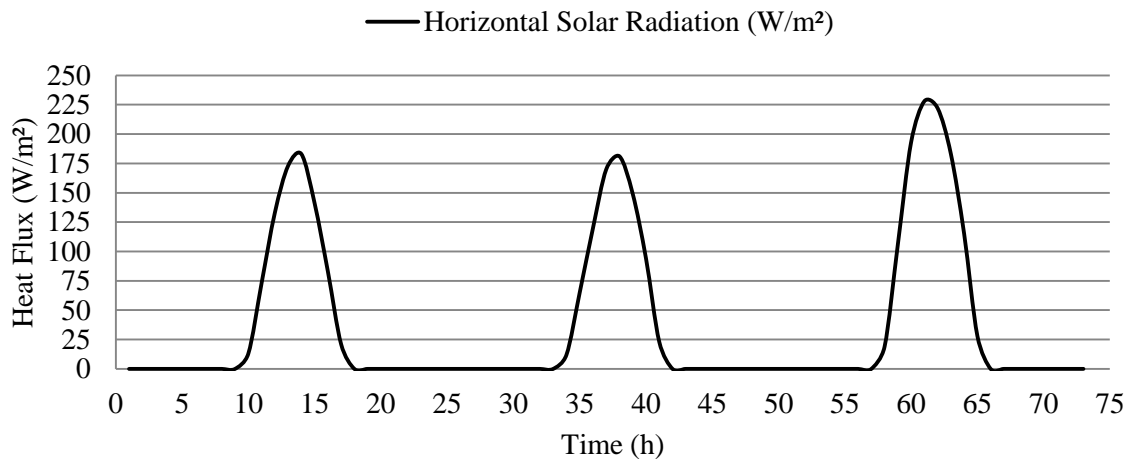
Figure 15: Winter meteorological data-solar radiation for Victoria, Canada

To explain how the composite Trombe wall works in the heating season, a simulation with the above weather data was carried out for a closer look at this system. Figure 16 shows the time dependent temperature distribution in the wall. The shade area in the plot indicates the night hours (without solar radiation). At 9 a.m. on December 21st, once the sun comes out, the exterior glazing starts gaining solar heat immediately, while the Trombe wall is still in a warm-up stage. Around 11 a.m., the accumulated heat in the wall gets saturated and there is heat flux going through the inner surface of the mass wall, which leads to the temperature rise on that surface. At 1p.m., the atmosphere solar radiation comes to its peak value when the

Trombe wall is still taking in heat until it reaches the highest value at 1:30. After the peak point, solar radiation goes down while the Trombe wall discharges. Heat flux into the interior continues even after sunset at 5 p.m. The room temperature hits the highest point at 8:30 in the evening. This discharging process provides heat to the living space until the next morning when the sun rises again.
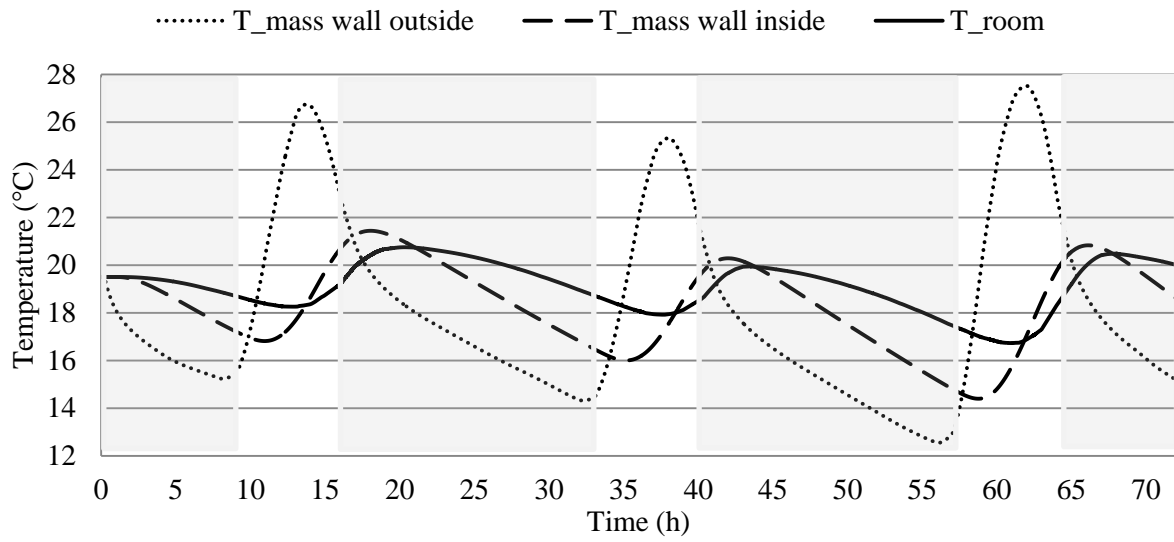
Figure 16: Time dependent temperature distribution within the wall

With the composite Trombe wall passive heating during the day and the mass wall's thermal storage ability, the indoor average air temperature rises to between 17°C and 21°C, as shown in Figure 16.
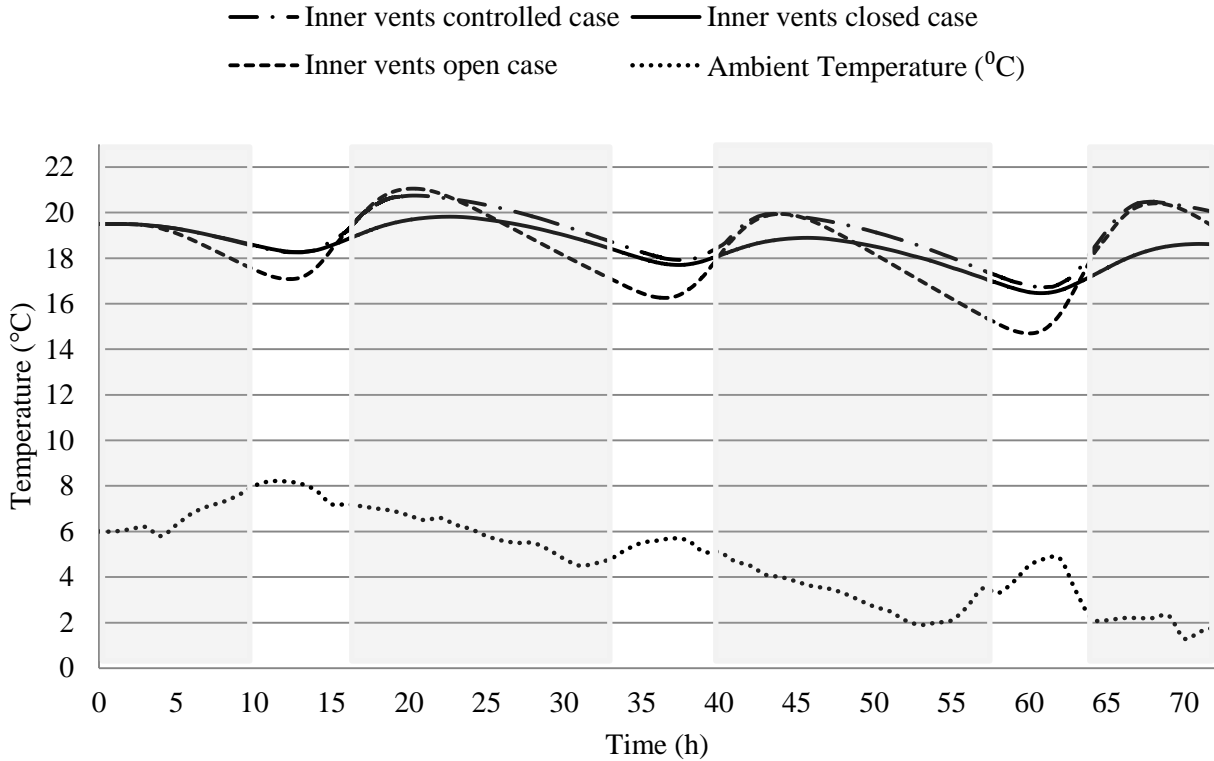
Figure 17: Average air temperature in the room under the influence of vents in winter

One of the advantages of the composite Trombe wall is that its vents on the interior insulation panel can be closed at night to prevent reverse air circulation. Figure 17 shows the effect of the vents on the indoor air average temperature (T_r). The shade area in the plot indicates the night hours (without solar radiation). With open vents, T_r fluctuates between 14.7°C and 21.2°C. According to the West Midlands Public Health Observatory, the adequate level of wintertime warmth is 18.5°C with 22°C as a maximum comfortable room temperature for sedentary adults [23]. In this case, there are 34.8 hours out of 72 hours where T_r is lower than 18.5°C.

In the case of closed vents, T_r has much less fluctuation with a minimum temperature of 16.5°C and a maximum of 19.8°C. The number of hours below 18.5°C drops to 29.8 hours.

With controlled vents, the vents will be closed once there is reversed flow. Heat will be blocked inside and prevented from leaking when T_r is higher than the wall temperature. This results in only 18.3 hours out of three days when T_r is below 18.5°C. If more heat gained

during the day transfers into the interior, instead of losing to the ambiance through the glazing, the number of hours when T_r is lower than 18.5°C will be further reduced. This indicates that the model from the published research, which is based on the climate of France, doesn't perform as well in Victoria's climate. Structural optimization is required to make the wall achieve better interior comfort level.

4.2 Cooling Season

Figure 18 and Figure 19 show the summer weather data (June 20-22) for cooling season simulation. Within these three days, the ambient temperature ranges from 14°C to 24.5°C with abundant solar radiation, which may lead to over-heating during the day.
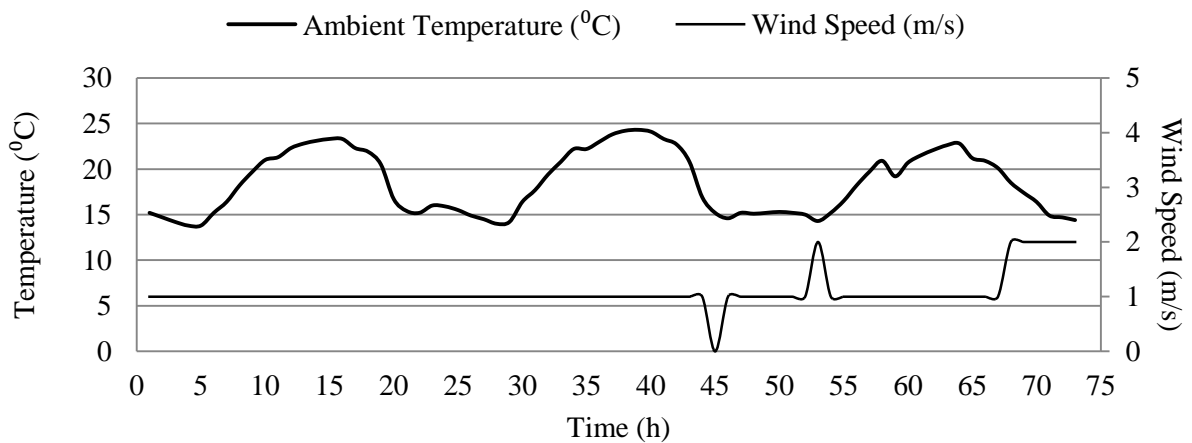
Figure 18: Summer meteorological data-temperature and wind speed for Victoria, Canada
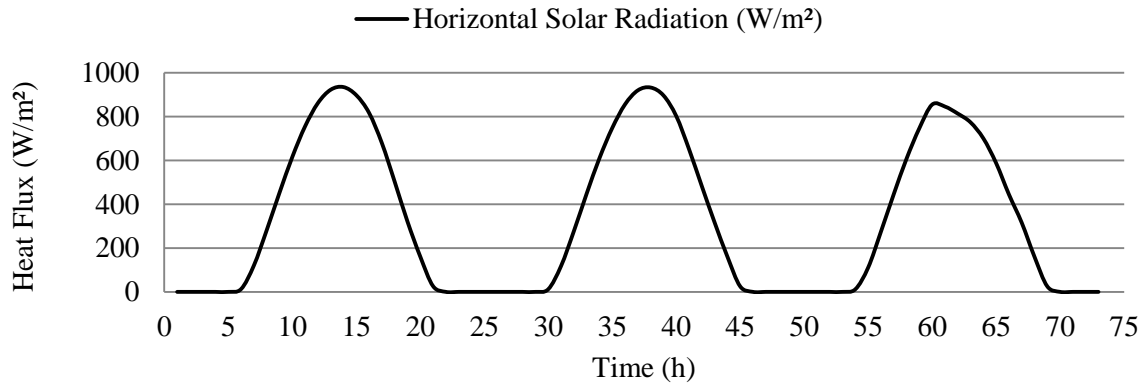
Figure 19: Summer meteorological data-solar radiation for Victoria, Canada

In the summer time, the abundant solar radiation can potentially cause serious over-heating issues for passive houses. In this case, as shown in Figure 21, even when the interior vents on the insulation wall are closed to block heated air ventilation, the average room temperature still unacceptably reaches at 80°C.

In order to cut off the extra heat going into the system, two ventilation vents are mount to the top and bottom of the glazing gap respectively, as shown in Figure 20.
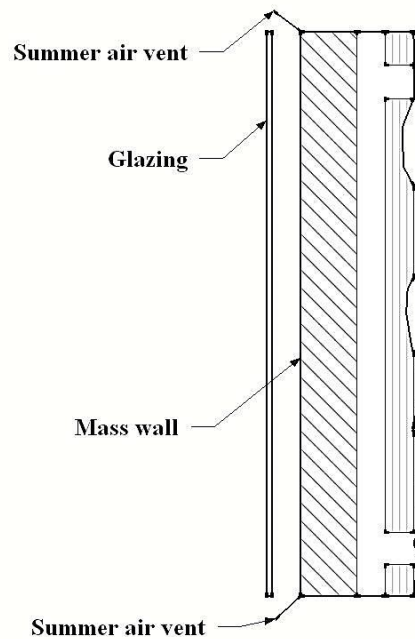
Figure 20: Schematic of exterior vents for summer

With the exterior vents open for cooling the solar collector surface (outside mass wall surface) and the interior vents closed to block extra heat away from the living space, the indoor average air temperature stays between 17.8°C and 19.4°C, as shown in Figure 21. The shade area in the plot indicates the night hours (without solar radiation).
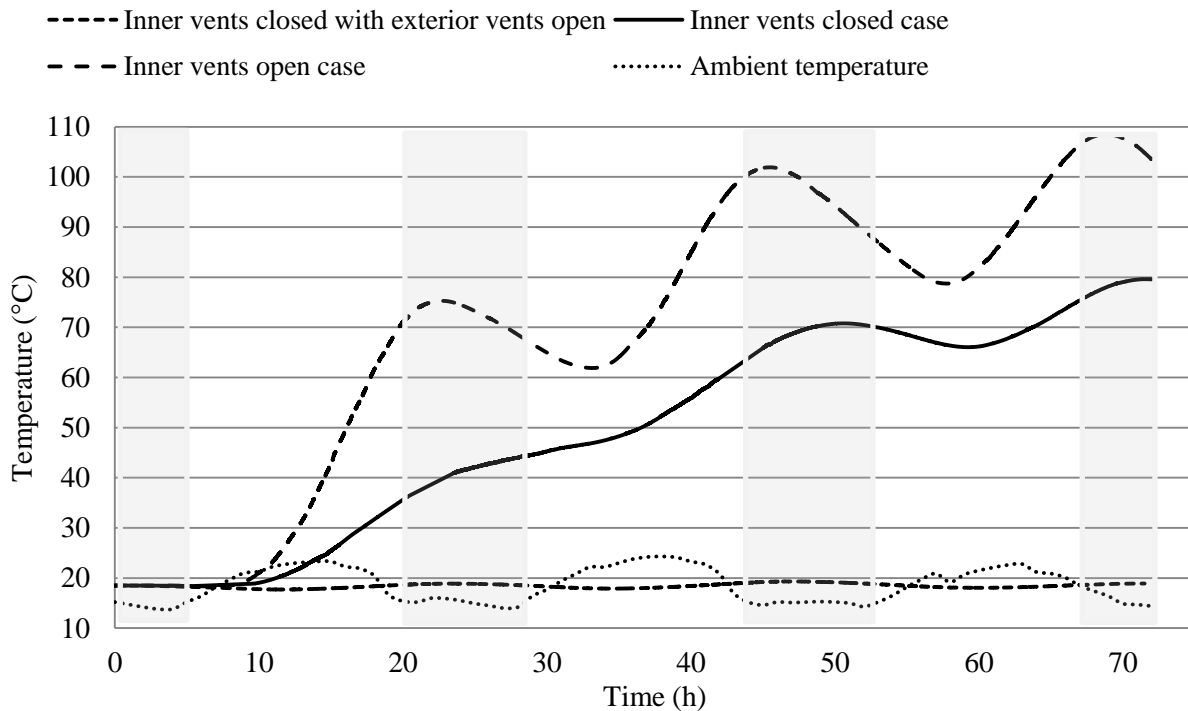
Figure 21: Average air temperature in the room under the influence of interior and exterior vents in summer

While the above model provides certain heating and cooling ability, with the model adopted directly from the published paper, insufficient heating occurs during the winter time. This requires some modification of the existing model to adapt to Victoria's climate. Optimization of the structural parameters will be studied in the next section.

Chapter 5   Trombe Wall Parametric Study

A two step-parametric study was conducted to determine energy-optimal design configurations for the composite Trombe wall system. Various design configurations were modeled and analyzed for heating application with the aim of providing the indoor comfort without any active heating at all while reducing the temperature gradient to a minimum.

The first step will modify four parameters of the wall structure to achieve better average indoor temperature with Victoria's typical weather data. Based on the first simulation result, the second study will focus on optimizing three factors of the ventilated air channel between the mass wall and insulation wall, in order to reduce the temperature gradient at the human height level, creating a more comfortable dwelling environment for occupants.

Based on the experience in validation stage, each simulation of the whole system takes about two hours to finish. If a full factorial parametric study is conducted, for example, a study of four factors, each with three potential values, 81 simulations have to be processed. This requires a lot of calculation resources. Therefore, finding a proper way to sample the design space is necessary.

5.1 Study One

In the first step, the following four parameters, each with different levels of value, will be studied to find an optimal modified design:

- the thickness of the mass wall (L_m),

- the thickness of the insulation wall (L_i),

- the size of the interior vents (H_v),

- the emissivity of the glass layer(ε).

5.1.1 Selecting Orthogonal Array

When designing certain experiments to assess the influence of multiple input parameters on one or more output parameters, there are different statistical techniques to find a way to sample the design space. One of them is called orthogonal array (OA) method. Compared to a full-factorial design, orthogonal array technique helps in creating a concise test set with many fewer test cases than testing all combinations of all variables which would consume much more time. It reduces the number of simulations while still able to capture the important effects by finding the best coverage of the design space. [24]

These variables are called *factors* and the whole set of possible values for each factor is called *levels*. In this case, as presented in Table 3, there are four factors that are designated as A, B, C, D. Each factor has three levels: lower value, mid value and higher value.

Table 3.Study 1 - Selected process parameters and respective levels in the experimental design

Parameters	Designation	Level 1	Level 2	Level 3
Thickness of the mass wall (L_m)/m	A	0.1	0.15	0.2
Thickness of the insulation wall (L_i) /m	B	0.05	0.075	0.1
Size of interior vents (H_v) /m	C	0.1	0.15	0.2
Emissivity of glass (ε)	D	0.07	0.33	0.9

Compared to a full-factorial design, which ends up with $81(3^4)$ combinations, the orthogonal array $L_9(3^4)$ only generates nine experiments to be conducted. Table 4 depicts the orthogonal array for this case, noted as $L_9(3^4)$. The first column is the layout numbers, or the experimental run number – 1 to 9 for the $L_9(3^4)$ array. It consists of four columns and nine rows and the numbers in rows and columns are 1, 2 and 3. By corresponding 3-level factors to columns, each row represents a trial condition with the level of factors. The column of values (P_i) on the right is for the experiment results of performance parameter.

Table 4.Study 1 - Experimental layout by $L_9(3^4)$ OA design

Experimental runs	A(3)	B(3)	C(3)	D(3)	Performance parameter values
1	1	1	1	1	P_1
2	1	2	2	2	P_2
3	1	3	3	3	P_3
4	2	1	2	3	P_4
5	2	2	3	1	P_5
6	2	3	1	2	P_6
7	3	1	3	2	P_7
8	3	2	1	3	P_8
9	3	3	2	1	P_9

When any of the two columns have numbers 1, 2 and 3 in nine combinations, (11), (12), (13), (21), (22), (23), (31), (32) and (33), occurring the same number of times, the two columns are considered to be "balanced" or "orthogonal", which means the inner product of vectors corresponding to weights is zero. [25] If the three levels are normalized between -1 and 1, the weighting factors for these levels are -1, 0, 1 respectively. Take variable 2 and variable 4 for example, the inner product of these two columns would be

$$[(-1) \times (-1) + 0 \times 0 + 1 \times 1] + [(-1) \times 1 + 0 \times (-1) + 1 \times 0] \qquad (5.1)$$
$$+ [(-1) \times 0 + 0 \times 1 + 1 \times (-1)] = 0$$

Table 5.Study 1 - Experimental layout with the variables in their original units

Experimental runs	Factor (levels)			
	Thickness of mass	Thickness of insulation	Size of interior	Emissivity of glass
1	0.1	0.05	0.1	0.07
2	0.1	0.075	0.15	0.33
3	0.1	0.1	0.2	0.9
4	0.15	0.05	0.15	0.9
5	0.15	0.075	0.2	0.07
6	0.15	0.1	0.1	0.33
7	0.2	0.05	0.2	0.33
8	0.2	0.075	0.1	0.9
9	0.2	0.1	0.15	0.07

5.1.2 Wall Parameter Study Results

Based on the heating season results in section 4.1, there were still 18.3 hours when T_r is below 18.5°C even with the controlled interior vents. As the last simulation day (from 48h to 72 h) obtains 11.1 hours, over 60% of the under-heated hours, day 3 is chosen for the modification simulation.

The results of the experiments are obtained from simulation. Since the computer will always use the same calculation methods, which lead to same level of noise signal, only one run of simulation will be conducted for each array.

The performance parameter values (P_i) are the output of the simulations. They are calculated as the sum of squared deviation of the half-hourly average indoor temperature from the middle value of comfortable indoor temperature range (19.75℃):

$$P_i = \sum (T_r - 19.75)^2 \qquad (5.2)$$

Using the parametric sweep function in COMSOL Multiphysics®, the nine numerical simulations are carried out with the validated model. The results of the simulations are shown in Table 6.

Table 6.Study 1 - Performance parameter results from simulations

| Experimental | Factor (levels) | | | | Performance |
runs	A(3)	B(3)	C(3)	D(3)	parameter values
1	1	1	1	1	P_1=462.26
2	1	2	2	2	P_2=255.49
3	1	3	3	3	P_3=134.37
4	2	1	2	3	P_4=61.03
5	2	2	3	1	P_5=103.87
6	2	3	1	2	P_6=55.30
7	3	1	3	2	P_7=21.10
8	3	2	1	3	P_8=36.49
9	3	3	2	1	P_9=19.30

5.1.3 Analysis of Variance

Once the experiments are conducted, the Analysis of Variance (ANOVA) is performed to segregate the main effect of each individual factor. The ANOVA evaluates the significance of the factors by calculating the mean value of each level of a design factor (M), sum of square value of the design factor (SSV), total sum of square (TSS), percentage contribution (PC) and near optimal level value (NOLV).

5.1.3.1 Mean value of each level of a design factor (M)

The mean value of each level of a particular factor is generated by dividing the sum of the performance parameter values, which are attributed by a particular level, with the number of replications of this level. For example, the mean value of level 3 for factor 4 is given by:

$$M_{43} = \frac{(P_3 + P_4 + P_8)}{3} \tag{5.3}$$

Table 7 shows the mean values of each level of the four design factors:

Table 7.Study 1 - Mean values of each level for the four design factors

	Lm	Li	Hv	ε
level1	284.04	181.46	184.68	195.05
level2	73.40	131.95	111.85	110.63
level3	25.54	69.57	86.45	77.30

When the thickness of the mass wall and the insulation wall, the size of the interior vents and the emissivity of glazing are increased, the M value reduces. This means the average indoor temperature fluctuates less around the mid-value of comfort zone. The following analysis will tell, among these factors, which one plays a more important role in stabilizing the indoor temperature.

5.1.3.2 Sum of the square value of the design factor (SSV)

The sum of the square value of a factor is calculated using the following equation:

$$SSV_i = R \times \sum_{j=1}^{Le} (\bar{M} - M_{ij})^2 = \frac{\sum_{j=1}^{Le} A_i^2}{R} - \frac{S^2}{N} \qquad (5.4)$$

where Le is the number of the level, R is the number of repetitions per level, N is the total number of experiments conducted, S is the sum of observations of all the experiments determined by

$$S = \sum_{i=1}^{N} P_i \qquad (5.5)$$

A_i is the sum of all observations of level i of the factor, $\bar{M}$ is the grand mean value of all the experiments determined by:

$$\bar{M} = \frac{S}{N} \qquad (5.6)$$

and M_{ij} is the mean value of jth level of ith factor.

Take the sum of square value of factor 2 for example:

$$SSV_2 = \{[\bar{M} - \frac{(P_1 + P_4 + P_7)}{3}]^2 + [\bar{M} - \frac{(P_2 + P_5 + P_8)}{3}]^2 + [\bar{M} - \frac{(P_3 + P_6 + P_9)}{3}]^2\} \times 3 \qquad (5.7)$$

$$= \frac{(P_1 + P_4 + P_7)^2 + (P_2 + P_5 + P_8)^2 + (P_3 + P_6 + P_9)^2}{3} - \frac{\left(\sum_{i=1}^{9} P_i\right)^2}{9}$$

The sum of the square value of the design factors (SSVs) are shown in Table 8.

5.1.3.3 Total sum of square (TSS)

The total sum of square is the sum of deviation of the observation values from the grand mean value, calculated by equation:

$$TSS = \sum_{i=1}^{N}(P_i - \bar{M})^2 = \sum_{i=1}^{N} P_i^2 - \frac{(S)^2}{N} \tag{5.8}$$

Due to the potential interaction effect between different factors (S_e), the TSS may not equal to the total sum of SSV of each factor. S_e is calculated as:

$$S_e = TSS - \sum_{i=1}^{K} SSV_i \tag{5.9}$$

where K is the total number of factors.

5.1.3.4 Percentage contribution (PC)

The percentage contribution of a certain factor is the ratio of the factor's SSV to TSS:

$$PC_i = \frac{SSV_i}{TSS} \tag{5.10}$$

This ratio indicates the influence of the factor over the performance parameter. The greater the value the more it contributes to the final results. Table 8 shows the PC for all the factors.

Table 8.Study 1 - Sum of square value and percentage

contribution for the four design factors

	Lm	Li	Hv	ε
Sum of Square Value	1.1e5	1.9e4	1.6e4	2.2e4
Percentage Contribution	67%	11%	9%	13%

It indicates that the thickness of the mass wall has the most influence over the indoor temperature with over two thirds of the contribution. The other three factors are equally important in determining the other 30% of comfort.

5.1.4 Near Optimal Level Value and Optimal Configuration

After figuring out the main influential factor, a new experiment should be conducted in order to find the near optimal level value (NOLV) of the performance parameter. In this experiment, the near optimal level for each design factor will be applied, which can be easily determined from the mean values of all the levels for each factor (Table 7).

By comparing the *M* value, the following levels in Table 9 are chosen as NOLVs. These values can be used as the initial value for further optimization. It is necessary to clarify that the NOLVs ending up all at level 3 of the four factors is coincident based on this method.

Table 9.Study 1 – Near optimal level value for the four design factors

Lm	*Li*	*Hv*	*ε*
level3	level3	level3	level3
0.2m	0.1m	0.2m	0.9

Though the near optimal level value combination is supposed to result in the best performance, sometimes this might not occur due to the interaction effect between different factors. What's more, as mentioned above, the fact that all NOLVs end up at level 3 implies that all the level 3 values might be potentially increased to achieve better results. A confirmation test will be implemented based on the estimated value for the near optimal condition, calculated by the following formula [26].

$$M_{optimal} = \overline{\text{M}} + \sum_{i=1}^{K} \omega_i \times [(M_o)_i - \overline{\text{M}}]$$

(5.11)

where $M_{optimal}$ is the optimal performance parameter which will be compared with the one calculated based on the optimal level values for each factor; K is the number of factors; $\overline{M}$ is the grand mean value of all the experiments; M_o is the near optimal level value for ith factor which is based on Table 7; ω_i is the weight for each factor depending on its significance, which is determined by the following formula:

$$\omega = 0 \qquad when \; F = \frac{MSV}{MSE} \leq 1 \tag{5.12}$$

$$= 1 - \frac{1}{F} \quad when \; F = \frac{MSV}{MSE} > 1$$

where MSV is the mean sum of the square value of a design factor, MSE is the mean sum of the square of error. These two variables are given by:

$$MSV = \frac{SSV_i}{Le - 1} \tag{5.13}$$

$$MSE = \frac{TSS - SSV_i}{(N - 1) - (Le - 1)} = \frac{TSS - SSV_i}{N - Le} \tag{5.14}$$

where Le is the number of level, N is the total number of experiments conducted.

Based on the above formulas, the mean sum of square value, the mean sum of square of error and the weight for each factor are shown in Table 10.

Table 10.Study 1 - Mean sum of square value, mean sum of

square of error and weight for each factor

	Lm	Li	Hv	ε
MSV	5.7e4	9.4e3	7.8e3	1.1e4
MSE	9.4e3	2.5e4	2.5e4	1.1e4
ω	0.9	0	0	0.4

The estimated optimal performance parameter is calculated in Equation (5.15)

$$M_{optimal} = \overline{M} + \sum_{i=1}^{K} \omega_i \times [(M_o)_i - \overline{M}] = 15.02 \tag{5.15}$$

A confirmation simulation is set up with the near optimal level values from Table 9. Based on the simulation result, the performance parameter value of this near optimal conditioned model is calculated as 13.53, with 9.9% deviation from the estimated optimal value. The optimal condition is acceptable.

To further look into how the optimal condition improves on the average indoor temperature, the comparison between the optimized model results and the results from cases of Orthogonal

Array trial, shown in Figure 22. To simplify the graph, only experiment No.7 and No. 9 which are the best performance cases among the total 9 runs, are demonstrated here. The shade area in the plot indicates the night hours (without solar radiation).
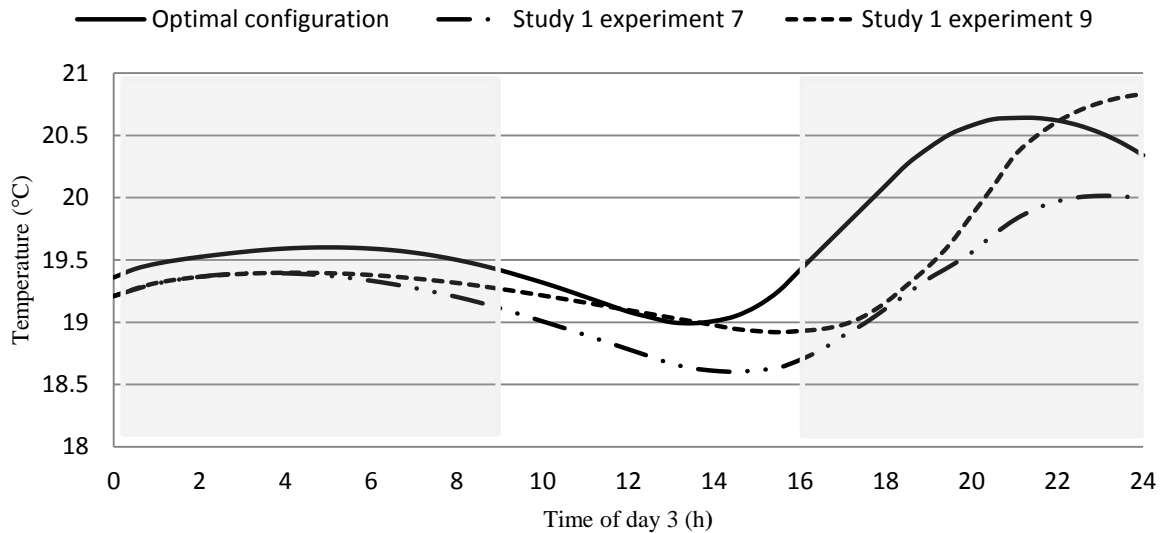

Figure 22: Study 1–Average indoor temperature generated from the optimized model, compared with two cases from OA trial

Compared to the other two cases, the optimized model generates less fluctuation in indoor temperature. The lowest temperature is 19°C, and the highest temperature is 20.64°C, which lies well within the range of comfort zone. Thanks to the high emissivity of the exterior glazing, the extra heat gathered during the day by the absorbing surface of the mass wall is able to be released back into the environment at night, which helps to avoid over-heating the room.

For most cases of passive house everywhere else in the world, the low emissivity glazing is one of the basic design elements, which helps to keep heat (long-wave infrared energy) inside in winter and blocks heat from the exterior during summer. However, in the case of Victoria, BC, its winter temperature is mild with enough solar radiation to raise the indoor temperature to the comfort level, especially with a thicker massive wall and an insulation panel. Extra low emissivity will only lead to over-heating in the interior even during the winter time. Therefore,

a regular single pane glazing with emissivity around 0.9 will fulfill its task to stabilize the indoor temperature at the human comfort level.

5.2 Study Two

By modifying the emissivity of glazing, the thickness of walls and the size of interior vents, the indoor spatial average temperature is achieved to be at a relatively best range. However, to determine the conditions for thermal comfort in the occupied space, other factors need to be considered. The main factors include temperature gradient, air velocity, air humidity, clothing insulation and activity level of the occupants [27]. The following study will investigate the temperature gradient in the room to achieve better indoor comfort level based on the first study above.

Vertical air temperature difference and draft often cause cold discomfort on the foot, ankle and leg [28]. To avoid such discomfort, the ASHRAE Standard 55 [29] recommends the vertical temperature difference between ankle level from the floor (0.1m) and head level (1.7m) should be less than 3°C, which leads to a temperature gradient at $1.875℃/m$ maximum.

In study 1, within the optimal configuration model, temperature values are collected by three sets of probes which are located at the very left, middle and right side of the dwelling space. Each set has two probes placing at 0.1m and 0.7m respectively. The average indoor air temperature gradient between 0.1m and 1.7m during the last day is calculated and shown in Figure 23. The shade area in the plot indicates the night hours (without solar radiation).
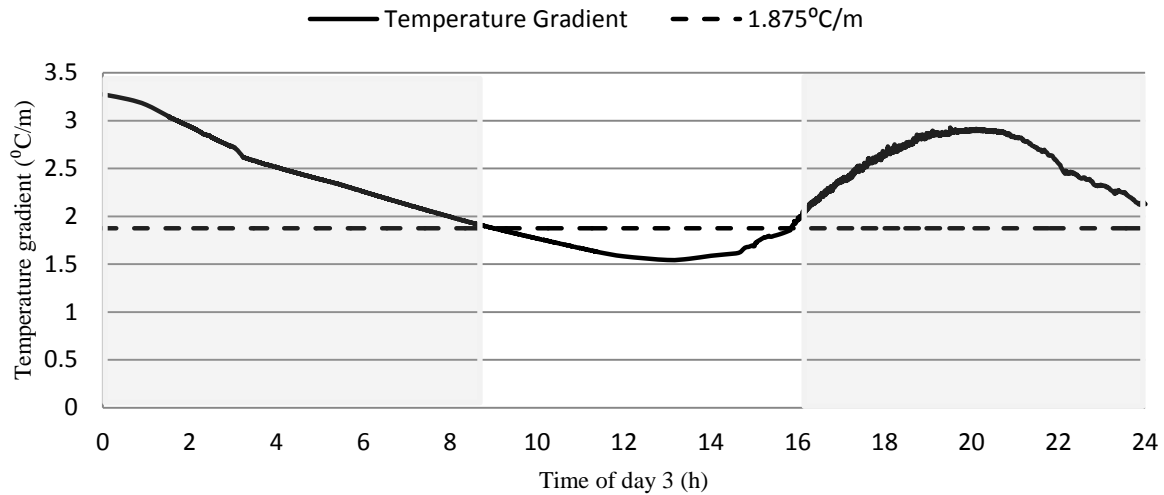
Figure 23: Study 2 - Indoor air temperature gradient between 0.1m and 0.7m during the last day of the optimized model from study one

Based on the optimized model from study 1, there are over 17 hours when temperature gradient is greater than $1.875°C/m$. During the early morning, and from late afternoon till midnight, the residents in the room will feel the cold and may be uncomfortable, and may even experience a slight breeze caused by the vertical temperature difference. Minimizing the hours of local discomfort will increase the dwelling's thermal comfort.

A second parametric study is conducted to investigate some of the structure parameters that influence temperature gradient, and find the optimized final design. Three parameters related to the interior vents and the ventilated air channel between the mass wall and insulation panel are studied:

- the thickness of the air channel between the mass wall and the insulation panel (L_2),

- the distance between the interior vents and the floor or the ceiling (H_f),

- the size of the interior vents (H_v).

5.2.1 Selecting Orthogonal Array

In the second experimental design, there are three factors, each with three levels, as presented in Table 11.

Table 11.Study 2 - Selected process parameters and respective levels in the experimental design

Parameters	Designation	Level 1	Level 2	Level 3
Thickness of ventilated air layer (L_2) /m	E	0.02	0.04	0.06
Vents location from floor level (H_{fl}) /m	F	0.035	0.085	0.135
Size of interior vents (H_v) /m	G	0.18	0.2	0.22

Orthogonal array technique is applied here again to generate the trial conditions. Compared to a full-factorial design, which ends up with 27 combinations, orthogonal array L_6 gives six experiments to be conducted. Table 12 below depicts the new array.

Table 12.Study 2 - Experimental layout by $L_6(3^3)$ OA design

Experimental runs	Factor (levels)			Performance parameter values
	E(3)	F(3)	G(3)	
1	1	2	2	P_1
2	2	1	3	P_2
3	3	3	3	P_3
4	1	2	2	P_4
5	2	3	1	P_5
6	3	1	1	P_6

If the three levels are normalized between -1 and 1, the inner product of any of the columns would be zero. Take factor F and G for example, the inner product is calculated as:

$$0 \times 0 + (-1) \times 1 + 1 \times 1 + 0 \times 0 + 1 \times (-1) + (-1) \times (-1) = 0 \qquad (5.16)$$

which confirms the array chosen is orthogonal.

Table 13 shows the array with the variables in their original units.

Table 13.Study 2 - Experimental layout with the variables in their original units

Experimental runs	Factor (levels)		
	Thickness of ventilated air layer (L_2) /m	Vents location from floor level (H_{fl}) /m	Size of interior vents (H_v) /m
1	0.02	0.085	0.2
2	0.04	0.035	0.22
3	0.06	0.135	0.22
4	0.02	0.085	0.2
5	0.04	0.135	0.18
6	0.06	0.035	0.18

5.2.2 Wall Parameter Study Results

Six simulations are carried out in COMSOL Multiphysics® with different levels of combinations of factors, as shown in Table 14. The outputs of the simulations are the performance parameter values (P_i). P_i is measured as the number of hours during the chosen day when the temperature gradient is greater than 1.875℃/m. The goal of this study is to minimize this parameter value.

The results of the simulations are shown in Table 14.

Table 14.Study 2 - Performance parameter results from simulations

Experimental runs	Factor (levels)			Performance parameter values
	E(3)	F(3)	G(3)	
1	1	2	2	P_1=16.5
2	2	1	3	P_2=12
3	3	3	3	P_3=15
4	1	2	2	P_4=16.5
5	2	3	1	P_5=17
6	3	1	1	P_6=13

5.2.3 Analysis of Variance

As in study 1, the Analysis of Variance (ANOVA) is performed to segregate the main effect
of each individual factor. The mean value of each level of a design factor (M), sum of square
value of the design factor (SSV), total sum of square (TSS), percentage contribution (PC) and
near optimal level value (NOLV) are calculated.

5.2.3.1 Mean value of each level of a design factor (M)

Table 15 shows the mean values of each level of the three design factors:

Table 15.Study 2 - Mean values of each level for the design factors

	L_2	H_{fl}	Hv
level1	16.5	12.5	15
level2	14.5	16.5	16.5
level3	14	16	13.5

5.2.3.2 Sum of square value of the design factor (SSV)

Using the same method, the sum of observation of all the experiments (*S*) is used to calculate
SSV. The only difference is the total number of experiments conducted (*N*).

The results are shown in Table 16.

5.2.3.3 Total sum of square (TSS)

This value is used to evaluate each factor's percentage contribution.

$$TSS = \sum_{i=1}^{N}(P_i - \bar{M})^2 = \sum_{i=1}^{N} P_i^2 - \frac{(S)^2}{N} \tag{5.17}$$

5.2.3.4 Percentage contribution (PC)

Table 16 shows the PC for the three factors.

Table 16.Study 2 - Sum of square value and percentage contribution for the design factors

	L_2	H_{fl}	Hv
Sum of Square Value	7	19	9
Percentage contribution	20%	54%	26%

Results indicate that the distance between the interior vents and the floor or the ceiling (H_{fl}) has the most influence over the indoor temperature field. Changing the location of vents on the insulation wall can significantly affect the fluid flow field in the dwelling, which will change interior heat distribution.

5.2.4 Near Optimal Level Value and Optimal Configuration

As the performance parameter has a smaller-the-better characteristic, the minimum mean value for each level of factor is chosen based on M. Table 17 summarizes these near optimal level values.

Table 17.Study 2 – Near optimal level value for the design factors

L_2	H_{fl}	Hv
level 3	level 1	Level 3
0.06m	0.035m	0.22m

A final simulation will be conducted based on the near optimal levels and the output performance parameter will be compared with the estimated optimal value calculated in the next step.

This confirmation test is to make sure the final model will result in the best indoor temperature field. The mean sum of square value, the mean sum of square of errors and the weight coefficient for each design factor are shown in Table 18.

Table 18.Study 2 - Mean sum of square value, mean sum of

square of error and weight for the design factors

	L_2	H_{fl}	H_v
MSV	3.5	9.5	4.5
MSE	9.3	5.3	8.7
ω	0	0.44	0

The estimated optimal performance parameter is calculated:

$$M_{optimal} = \overline{M} + \sum_{i=1}^{K} \omega_i \times [(M_o)_i - \overline{M}] = 11.49 \tag{5.18}$$

A confirmation simulation is set up with the near optimal level values from Table 17. Based on the simulation result, the hours with temperature gradient greater than $1.875°C/m$ is calculated as 11.7, with 1.8% deviation from the estimated optimal value 11.49. The optimal condition is proved to be acceptable.

Figure 24 shows the last day's temperature gradient in relation to the maximum temperature gradient allowed to achieve indoor thermal comfort. The shade area in the plot indicates the night hours (without solar radiation).
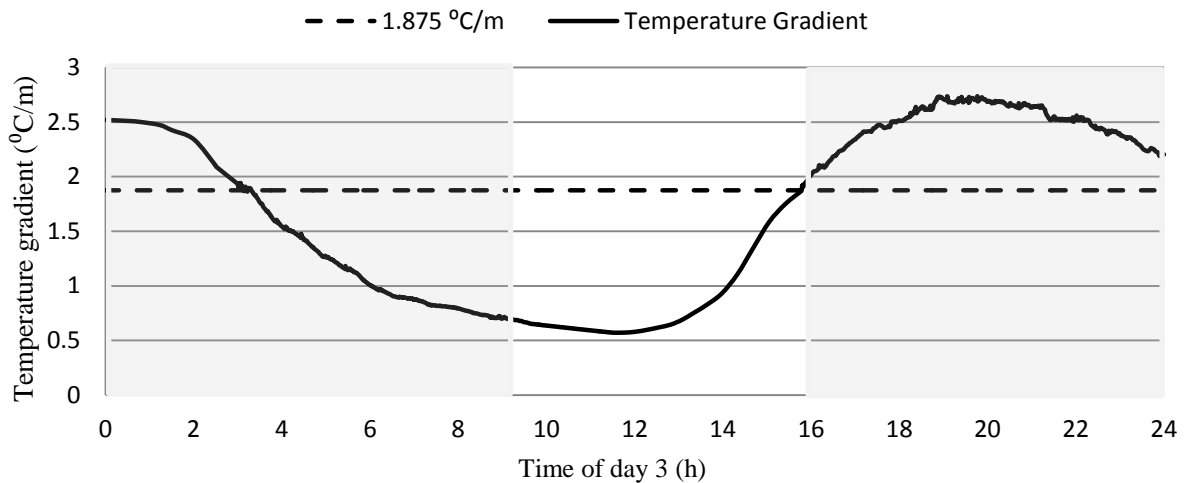
Figure 24: Study 2 - Indoor air temperature gradient between 0.1m and 0.7m during the last day of the optimized model from study two

In the first few hours, from midnight to 4 a.m. the wall structure (around 18°C) is cooler than the interior air (around 19°C), as shown in Figure 25-(b). As the exterior glazing temperature stays close to the ambient temperature at the moment (6°C), the total temperature difference throughout the whole structure will be 13°C. Plotting the whole structure's thermal map is not feasible if, COMSOL is used, as it will not be sensitive enough to show the detail of temperature gradient in the interior space. Therefore, only the room domain is plotted here.
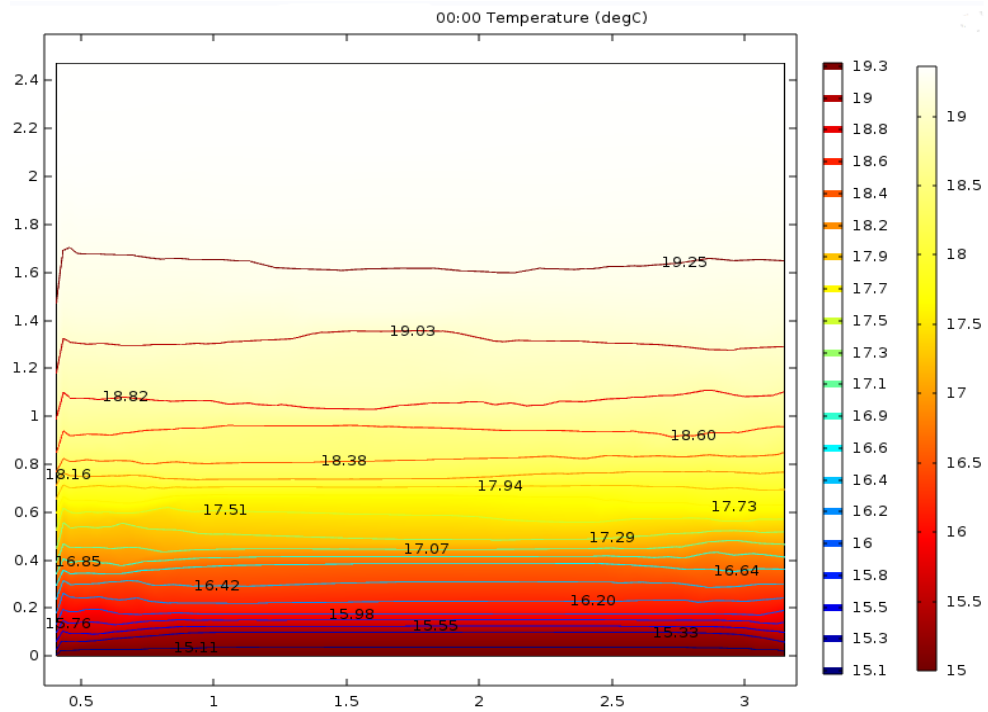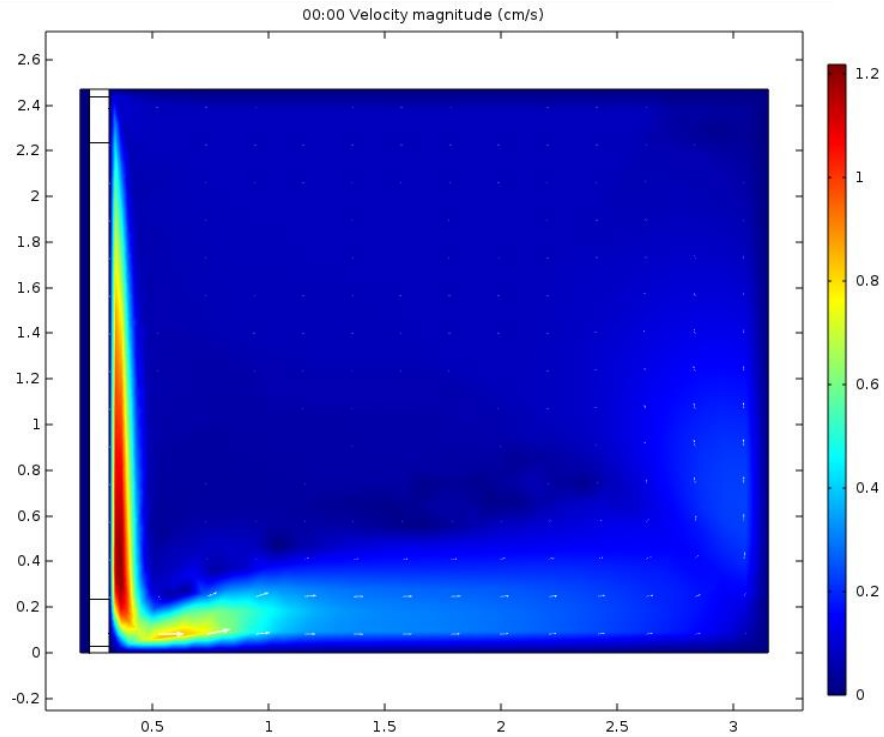
(a)

(b)

Figure 25: Study 2 - Time at 00:00. Magnitude of velocity (a) and temperature distribution map (b)

In the velocity magnitude map as demonstrated in Figure 25-(a), the air layer next to the wall's inner surface gets cooled down and sinks to the floor level. The white arrow in the map shows the velocity direction. This laminar flow leads to relatively high temperature stratification close to the floor. The air temperature in the upper space maintains uniform distribution.

Before the mass wall gets heated up again in the morning, the cold insulation wall keeps generating cooler sinking air, Figure 26-(a). As the cooler air accumulates, the indoor spatial temperature drops and tends to be more evenly distributed, as shown in Figure 26-(b).
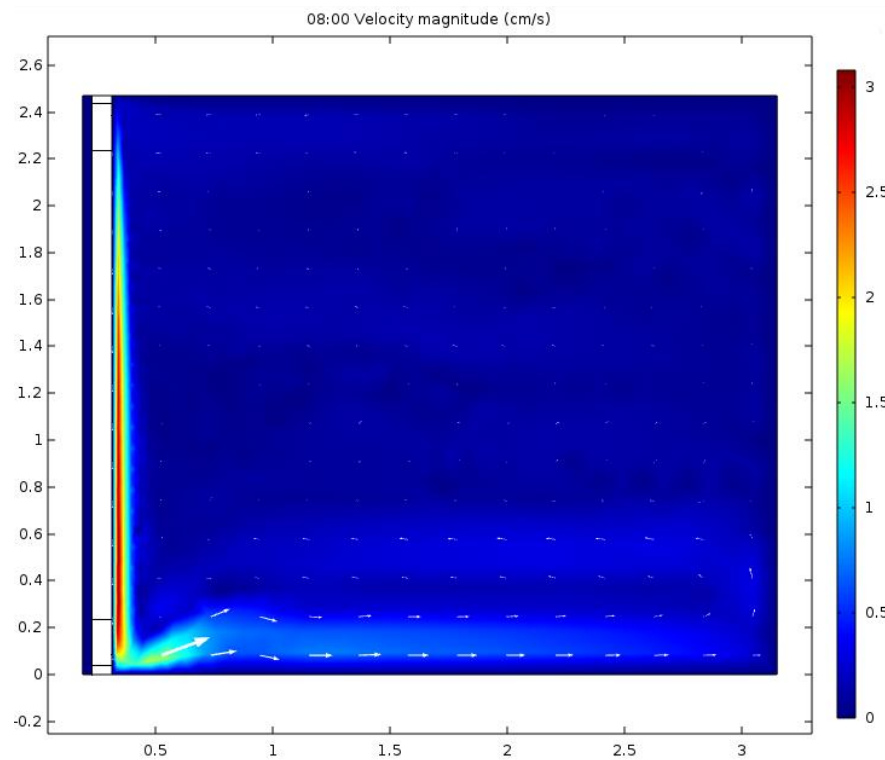

(a)
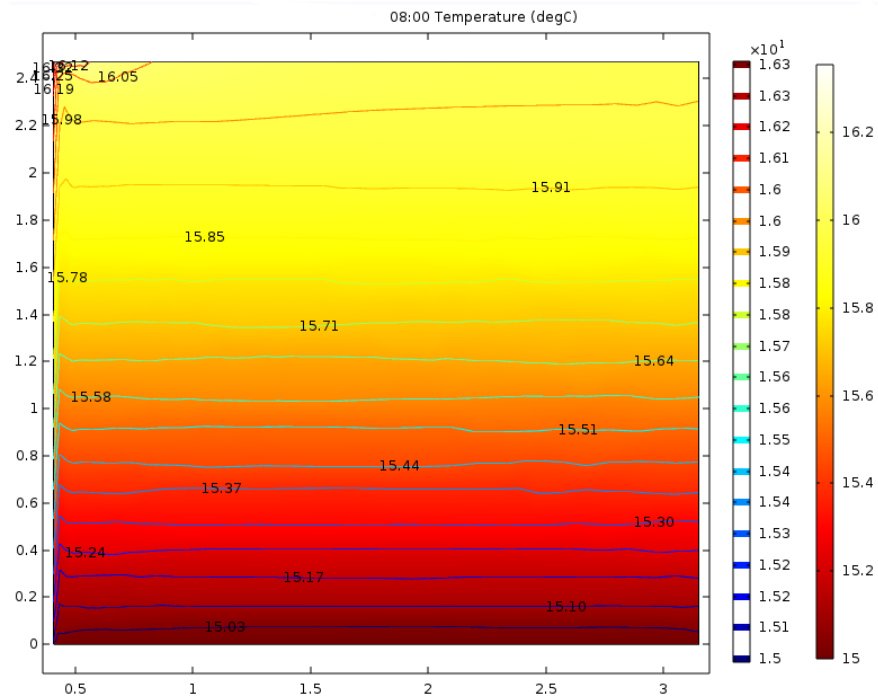
(b)

Figure 26: Study 2 - Time at 08:00. Magnitude of velocity (a) and temperature distribution map (b)

At around noon, the temperature gradient reaches its minimum value. By 11:30, the inside wall surface reaches the same temperature as the dwelling space, which means there won't be reversed air flow in the channel between the mass wall and insulation panel. Therefore, the interior vents are set up as open. The recharged storage wall starts heating up the air in the channel. Driven by the buoyancy force, the warm air goes into the room via the upper vent. The air closer to the ceiling gets warmed up sooner than the lower part, which results in higher temperature gradient, as indicated in Figure 27-(b). In the afternoon at 16:00, the air flow velocity in the ventilated channel reaches 4.8 cm/s, Figure 27-(a). Natural convection becomes the dominant heating method compared to the noon time, when conduction and radiation play a more important role, as the vents are just opened up and convection is weak at the beginning. Figure 27-(b) shows the temperature filed at 16:00.
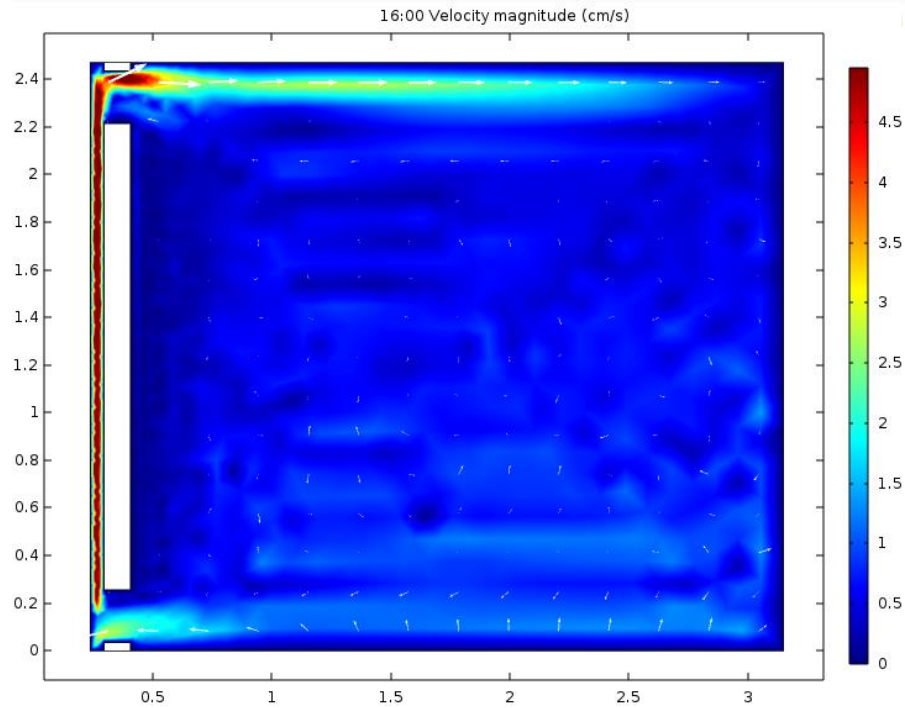
(a)
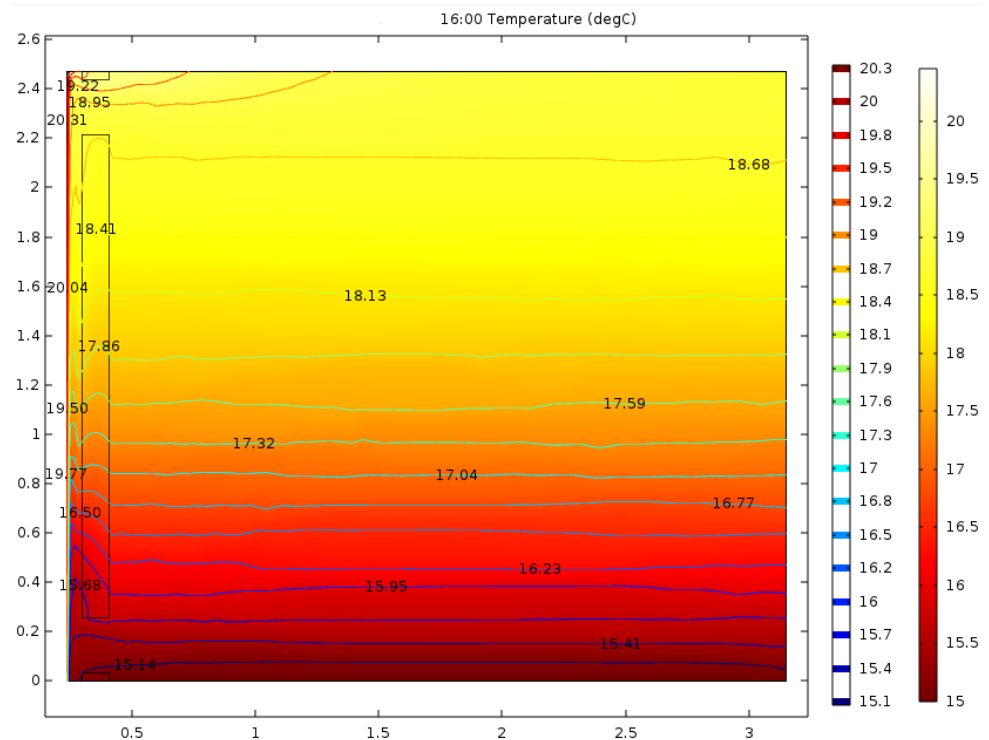
(b)

Figure 27: Study 2 - Time at 16:00. Magnitude of velocity (a) and temperature distribution map (b)

In the late afternoon and evening, as the mass wall gets saturated with thermal energy collected during the day, heat flux goes through the inner surface of the mass wall into the air channel. This leads to more severe air circulation through the channel and the dwelling space. At midnight, the natural convection still keeps heating up the interior air, though it slowly dies down, as shown in Figure 28-(a).
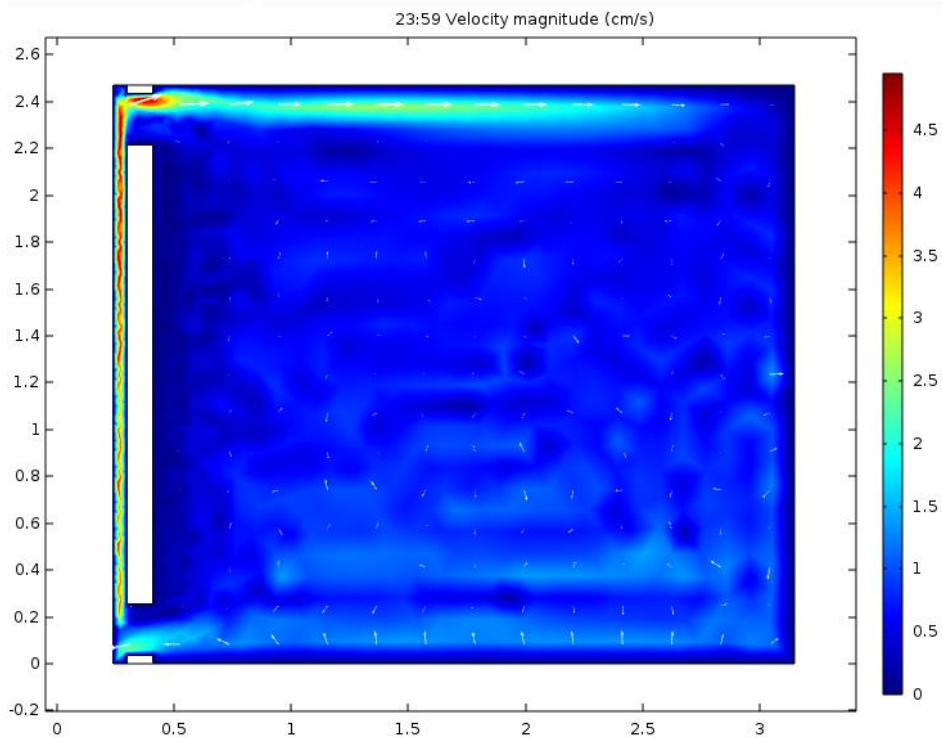

(a)
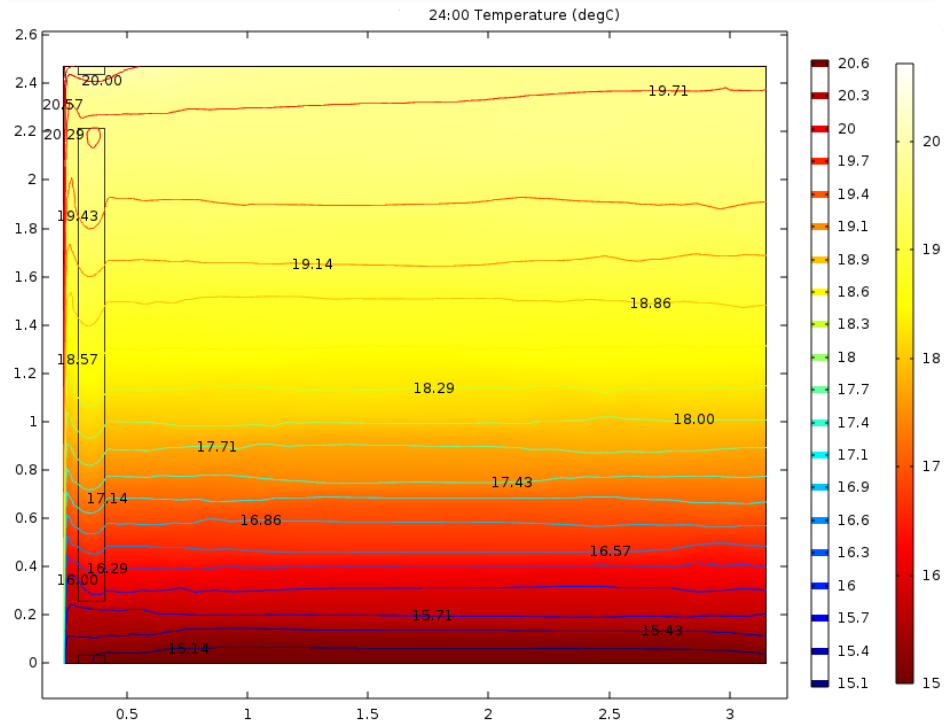
(b)

Figure 28: Study 2 - Time at 24:00. Magnitude of velocity (a) and temperature distribution map (b)

Taking a closer look at the four velocity magnitude maps throughout the day, at between 0.1m and 1.7m, the air velocity stays well below 15 cm/s at all times. According to ASHRAE 55, the ideal air velocity in the space should be kept to less than 15 cm/s during the heating season [29]. Even when it comes to more strict passive house standard, which requires a maximum air speed at 8cm/s [30], this composite Trombe wall model provides satisfying indoor comfort.
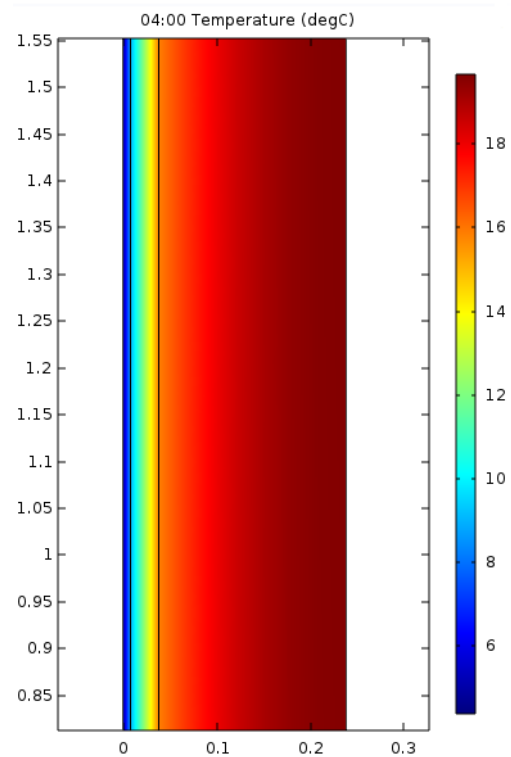
5.3   Demonstration of Thermal Storage Function of the Mass Wall

As mentioned before, due to the issue of plotting sensitivity of the simulation software, the glazing and mass wall layers are hidden from the thermal map. To give a full picture of the system and to better understand the interaction between the wall and the interior space, the passive heating and thermal storage function of the wall for the final modified model is demonstrated in the following seven figures. The plots show an amplified section of the wall. From left to right, the layers are glazing, sealed air gap, mass wall respectively.

The initial temperature is 20°C. At midnight, heat leaks into the environment through the glazing, Figure 29-(a). From 0:00 to around 9:00-when the sun starts rising on the winter solstice day- the mass wall keeps discharging captured heat. The closed-vent- insulation wall and the thick mass wall block the indoor heat to keep the interior warm at night, Figure 29-(b) and Figure 29-(c). Once the sun rises, the exterior surface starts heating up. The glass, sealed air layer and the mass wall create a mini greenhouse, trapping solar thermal energy behind the glazing. As shown in Figure 29-(d), the blackened mass wall exterior surface heats up first. At around noon, the vents of the insulation wall open up. Natural convection, driven by buoyancy, transfers heat into the interior. The massive wall keeps charging until sunset at 16:00, when it reaches its highest capacity, Figure 29-(e). Afterwards, the thermal energy travels through the wall and transfers to the dwelling space by convection via the channel, radiation and conduction via the insulation wall, as shown in Figure 29-(f) and Figure 29-(g).
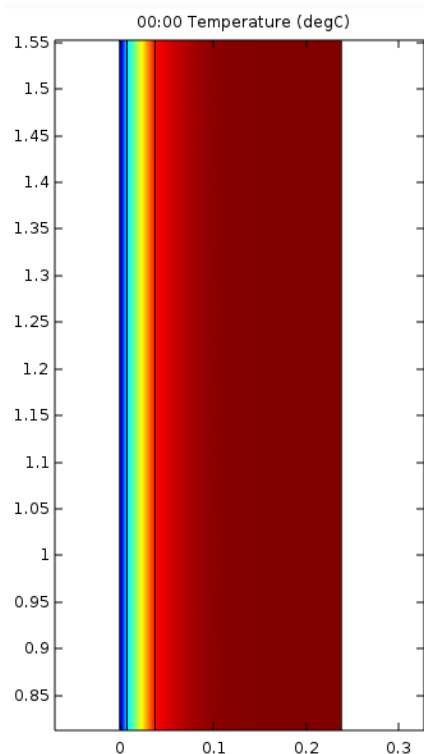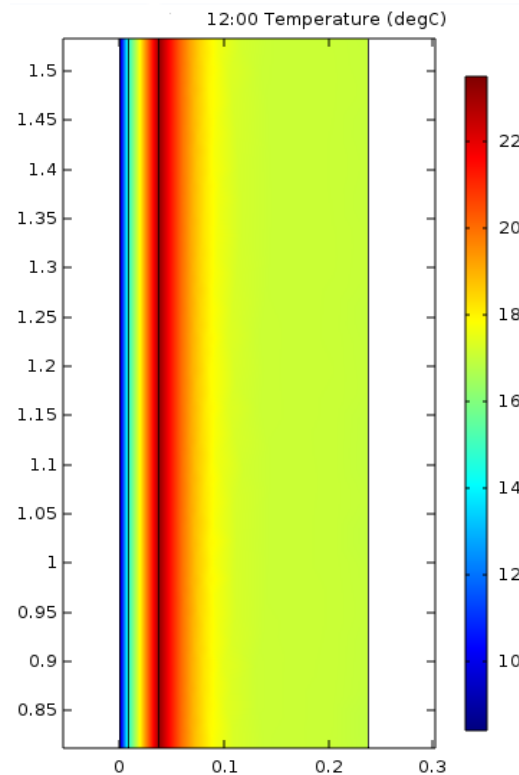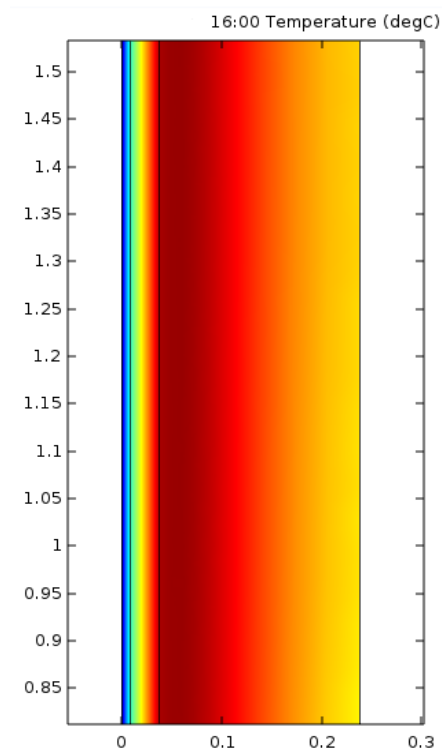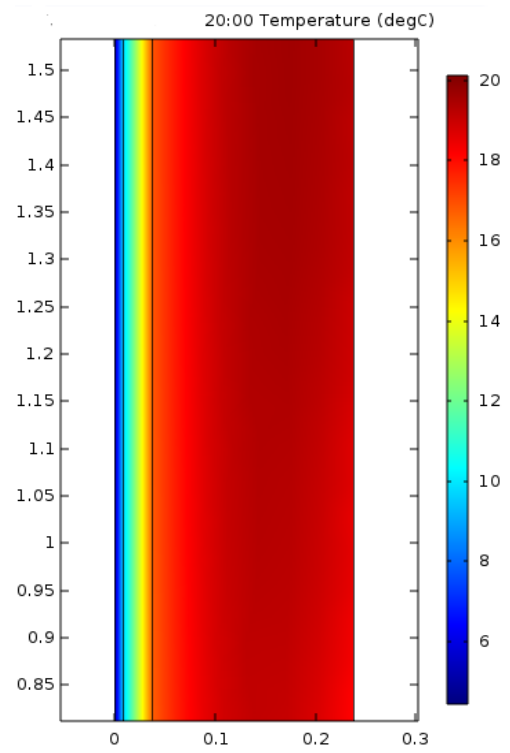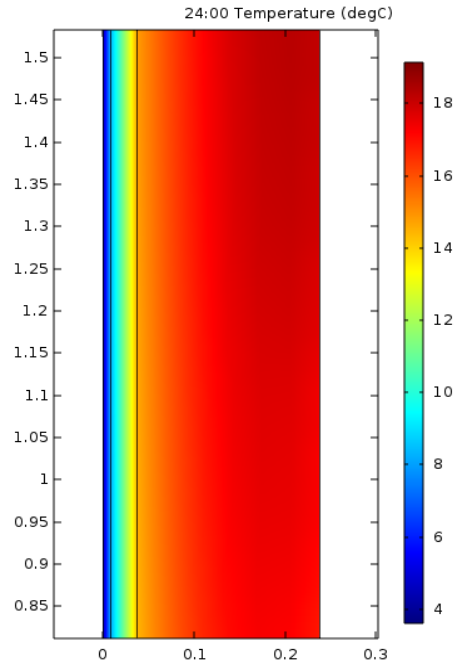

(a)

(b)
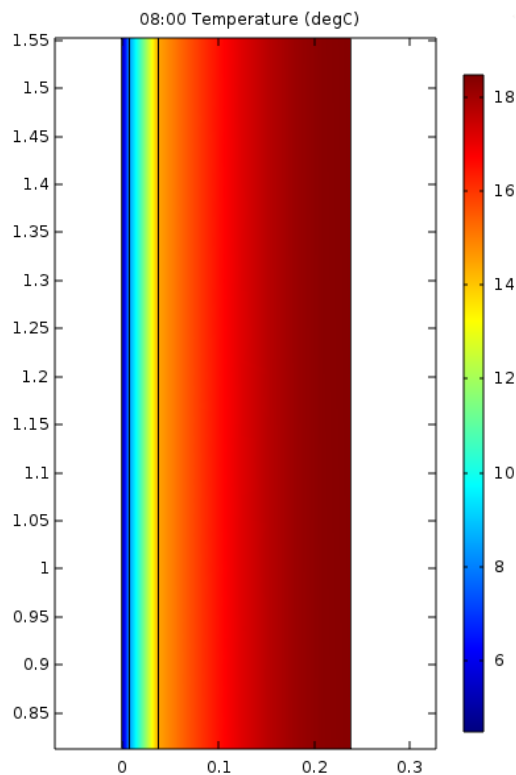
(c)

(d)

(e)

(f)

(g)

Figure 29: Demonstration of the passive heating and thermal storage function of the mass wall with the results from Study 2. Temperature field in mass wall at 00:00 (a); 04:00 (b); 08:00 (c); 12:00 (d); 16:00 (e); 20:00 (f); 24:00 (g)

5.4 Simulation Results

Two studies are carried out in order to modify the original model to adapt to Victoria's climate. Table 19 is a summary of all the parameters investigated and the optimized values for each parameter.

Table 19.Summary of both parameters studies

		Original model	Modified model	Changed by
Thickness of the mass wall	L_m	0.15m	0.2m	33%
Thickness of the insulation wall	L_i	0.075m	0.1m	33%
Emissivity of glass layer	ε	0.33	0.9	173%
Size of the interior vents	H_v	0.15m	0.22m	46%
Thickness of the air channel	L_2	0.04m	0.06m	50%
Distance to the floor or ceiling	H_{fl}	0.085m	0.035m	59%

The values of the parameters related to wall thickness (L_m, L_i, L_2), all increase. The vents get bigger and closer to the floor level. The emissivity value of glazing ends up so high that a regular single pane of glass can meet the requirement.

Compared to the original model created of the heating season, the first modified model from study one reduces the number of hours when T_r is below 18.5°C from 18.3 hours to zero. What's more, the optimized model generates less fluctuated indoor temperature which lies well within the range of the human comfort zone.

Based on the best-case model from study one, the second study improves the temperature stratification condition for the dwelling space. By increasing the air channel thickness, the size of the vents and lowering the vents to floor level, the second modification reduces the number of hours when temperature gradient is greater than 1.875°C/m from 17 hours to 11.7 hours (a reduction of 31%). Meanwhile, the air velocity in the dwelling space stays well below the maximum level designated by the Passive House Institute.

Since the optimized values of the six parameters hit either the upper or lower boundaries, expanding the variable ranges in order to achieve the best performance of the structure is suggested for the future study.

Chapter 6   Conclusion and Recommendation

This study concerns a numerical investigation into the thermal behavior of a composite Trombe wall and the modification of an existing model, adapting it to Victoria's local climate. Based on the validation of the model, both the heating and cooling mode of the structure were simulated. Insufficient heating ability during the winter requires modification to the existing model.

A two-step incremental design study with the orthogonal method reveals the main design parameters that affect the thermal performance of the passive heating system in winter. By setting up parametric studies for each investigation, the optimal value for each parameter was chosen for the modified final model.

Increasing the value of emissivity of glazing and the thickness of the mass wall and the insulation wall helps keep the indoor temperature in the thermal comfort zone for residents. By lowering the vent level, upsizing the air channel and vents, the indoor temperature is more evenly distributed, which further contributes to the level of indoor comfort.

Usually a low emissivity of glazing is preferable for passive houses. However, in this study, the mild winter in Victoria requires a relative high value of emissivity to stabilize the indoor temperature between 18.5°C and 22°C. Otherwise, over heating might occur with extra solar heat collected by glazing with a low emissivity value.

The other way to understand the relative high emissivity of the glazing is that there is possibility that the test case was essentially being overdesigned. This is a result of the available research data, which is only for a full size composite Trombe wall that covers the whole south-facing wall. In the case of Victoria, it is appropriate to design a composite Trombe wall partially covering the wall to avoid overheating as well as add in windows for daylighting.

The final modified model presented here is a result of theoretical simulation. To best fit the composite Trombe wall in Victoria, one needs to take some practical requirements, financial feasibility, local building codes and geographic condition into account. For example, the total

thickness of the passive heating wall is 40.8cm in the final design, which is much thicker than the regularly constructed exterior wall. The aesthetical influence and other potential effects from this untraditional building practice also need to be taken into account.

There are a number of areas for future investigation to modify the composite Trombe wall in order to better fit the west coast climate. First, for the sake of simplifying this model, the other walls of the room were assumed to be insulated. To make the numerical model generate better predictions of the indoor temperature field, heat transfer of these walls should be determined accurately. Second, after the final modification, there are still 11.7 hours of time when the temperature stratification can cause local discomfort for resident. Most of the higher gradient occurs in the morning and evening when residents are at home and require better thermal conditions. Third, as air humidity plays an important role on indoor comfort for the dwellers, future simulations should include this factor. There is evidence indicating the indoor temperature gradient is sensitive to the vent open/close schedule, and further numerical simulation can help to identify its role in the determination of the system performance and create an optimal schedule.

Reference

[1] *Passive House requirements*. (n.d.). Retrieved 10 30, 2015, from Passive House Institute: http://passiv.de/en/02_informations/02_passive-house-requirements/02_passive-house-requirements.html

[2] Asnaghi, A. &. (2012). Solar chimney power plant performance in Iran. *Renewable and Sustainable Energy Reviews, 16(5)*, 3383. doi:10.1016/j.rser.2012.02.017

[3] Fiaschi D, B. A. (2012). Design and exergy analysis of solar roofs: a viable solution with esthetic appeal to collect solar heat. *Renewable Energy* 46 (2012): 60-71.

[4] Onbasioglu, H., & Egrican, A.N. (2002). Experimental approach to the thermal response of passive systems. *Energy Conversion and Management, 43(15)*, 2053-2065. doi:10.1016/S0196-8904(01)00138-8

[5] Smolec, W., & Thomas, A. (1993). Theoretical and experimental investigations of heat transfer in a Trombe wall. *Energy Conversion and Management*, *34(5), 385-400*.

[6] A.K. Sharma, e. a. (1989). Vary-therm wall for cooling/heating of buildings in composite climate. *International Journal of Energy Research 13*, 733–739.

[7] L. Zalewski, M. C. (1997). Experimental thermal study of a solar wall of composite type. *Energy and Buildings 25*, 7–18.

[8] Shen, J. L. (2007). Numerical study of classical and composite solar walls by TRNSYS. *Journal of Thermal Science 16 (1)*, 46-55.

[9] Shen, J. L. (2007). Numerical study on thermal behavior of classical or composite Trombe solar walls. *Energy and buildings 39 (8)*, 962-974.

[10] Shen, J., Huange, D., Lassue, S., & Zalewski, L. (2006). Simulation of a Composite Solar Wall with the Finite Difference Method. *6th World Congress on Intelligent Control and Automation* (pp. Vol. 2, pp. 8789-8793). IEEE.

[11] Warner, J. L. (1995). Selecting windows for energy efficiency. *Home Energy*, 12(4).

[12] Dixon, J. (2008). *The Shock Absorber Handbook, Second Edition.* John Wiley & Sons.

[13] Jones, R. W. (1981). *Passive solar design handbook.* NM (USA): Los Alamos National Lab.

[14] *Handbook, ASHRAE. Fundamentals.* (2001). Atlanta: American Society of Heating, Refrigerating and Air Conditioning Engineers.

[15] ONG K.S, M. W. (1994). *Heat Transmission. 3rd ed.* New York: McGraw-Hill.

[16] G. D. Raithby, K. G. (1977). Analysis of heat transfer by natural convection across vertical fluid layers. *J. Heat Transfer*, 99, 287-293.

[17]   M. Fishenden, O. S. (1950). *An Introduction to Heat Transfer.* Oxford: Oxford University Press.

[18]   Yang S M, Z. Z. (1994). An experimental study of natural convection heat transfer from a horizontal cylinder in high Rayleigh number laminar and turbulent region. *10th International Heat Transfer Conference*, (pp. 7: 185-189). Brighton.

[19]   *COMSOL programming reference manual for Version: COMSOL 5.1.* (2015).

[20]   Griesmer, A. (2014, January 30). *Size Parameters for Free Tetrahedral Meshing in COMSOL Multiphysics*. Retrieved from COMSOL BLOG: https://www.comsol.com/blogs/size-parameters-free-tetrahedral-meshing-comsol-multiphysics/

[21]   Kottek, M. G. (2006). World map of the Köppen-Geiger climate classification updated. *Meteorologische Zeitschrift*, 15(3), 259-263.

[22]   *Victoria, British Columbia*. (n.d.). Retrieved from wikipedia: https://en.wikipedia.org/wiki/Victoria, British_Columbia#Climate

[23]   Hartley, A. (2006). *Fuel Poverty.* Birmingham, UK: West Midlands Public Health Observatory.

[24]   Box, G., & Hunter, W. a. (1978). *Statistics for Experimenters.* John Wiley & Sons.

[25]   Taguchi, G. &. (1993). *Taguchi methods: Design of experiments.* Dearborn, MI: ASI Press.

[26]   *Implementation of integrated approach for the development of infinite software* (n.d.). Retrieved from University of Massachusetts: http://www.ecs.umass.edu/mie/labs/mda/fea/sankar/chap5.html

[27]   *Designing for Comfort & IAQ: Air distribution*. (n.d.). Retrieved from constructionspecifier: http://www.constructionspecifier.com/designing-for-comfort-iaq-air-distribution-per-ashrae-55-and-62-1/

[28]   Melikov, A. K. (1989). Local thermal discomfort due to draft and vertical temperature difference in rooms with displacement ventilation. *1989 ASHRAE annual meeting* (pp. Volume: 95, Part 2). Vancouver: ASHRAE.

[29]   *Thermal environmental conditions for human occupancy, ASHRAE 55.* (2004). Atlanta,GA: ASHRAE.

[30]   *Thermal comfort parameters*. (n.d.). Retrieved from passipedia: http://www.passipedia.org/basics/building_physics_basics/thermal_comfort/thermal_comfort_parameters